ELSEVIER

Deep-Sea Research II 53 (2006) 718–740

DEEP-SEA RESEARCH
PART II

www.elsevier.com/locate/dsr2

Global POC concentrations from in-situ and satellite data

W.D. Gardner[a,*], A.V. Mishonov[a,b], M.J. Richardson[a]

[a]*Department of Oceanography, Texas A&M University, College Station, TX 77843 3146, USA*
[b]*National Oceanographic Data Center, 1315 East West Highway, Silver Spring, MD 20910 3282, USA*

Received 2 September 2004; accepted 30 January 2006

Abstract

During the last three decades significant contributions have been made to understanding regional and global distribution of chlorophyll in the ocean by developing algorithms from ocean-color products. Analogously, in this work empirical algorithms are developed to derive concentrations of particulate organic carbon (POC) from ocean-color products. We combined vertical profiles of particulate beam attenuation coefficient at 660 nm (c_p) collected on numerous cruises during World Ocean Circulation Experiment (WOCE), Joint Global Ocean Flux Study (JGOFS), South Atlantic Ventilation Experiment (SAVE), and other programs since the 1980s to create a global database. Discrete samples of POC and synchronously measured c_p data collected in the Atlantic, Pacific, Indian and Southern oceans during JGOFS and other programs were used to make c_p:POC regressions to convert c_p data to POC values. During the two programs, satellite data were available when synchronous POC samples and c_p profiles were obtained over several seasons. c_p averaged over one attenuation depth in the South Pacific and northeast Gulf of Mexico was correlated with four synchronous ocean-color products. A good correlation was obtained with both normalized water-leaving radiance at 555 nm ($L_{WN}(555)$) and diffuse attenuation coefficient at 490 nm (K_{490}). Using a combined K_{490}:c_p regression from the two areas, global maps of the estimated mean c_p were created and converted to mean POC concentration down to one attenuation depth for summer and winter seasons. Seasonal c_p, POC and chlorophyll distributions were used to map %CHL and c_p:CHL ratios within one attenuation depth as a possible index of phytoplankton physiology.

Keywords: Beam attenuation; Light transmission; Water transparency; POC; WOCE; JGOFS; SeaWiFS

1. Background and objectives

One of the major goals of the Joint Global Ocean Flux Study (JGOFS) was to develop regional and global mass balances for carbon. Various aspects of carbon budgeting have been attempted for selected areas through shipboard sampling during JGOFS Process and Time-Series Programs (e.g. North Atlantic Bloom Experiment (NABE)—Chipman et al., 1993; Arabian Sea—Lee et al., 1998; Equatorial Pacific—Walsh et al., 1995; Landry et al., 1997; Le Borgne et al., 2002; Antarctic Polar Front Zone—MacCready and Quay, 2001; Nelson et al., 2002; Ross Sea—Gardner et al., 2000a; Hawaii Ocean Time-Series (HOT)—Karl and Lukas, 1996; Bermuda Atlantic Time Series (BATS)—Steinberg et al., 2001). To extend global coverage, the marine carbon dioxide survey linked up with the World Ocean Circulation Experiment (WOCE) (Sabine et al., 2002; Feely et al., 2004).

*Corresponding author. Tel.: +1 979 845 7211; fax: +1 979 845 6331.
E-mail address: wgardner@ocean.tamu.edu (W.D. Gardner).

0967-0645/$ - see front matter © 2006 Elsevier Ltd. All rights reserved.
doi:10.1016/j.dsr2.2006.01.029

In order to make more complete carbon budgets it is necessary to know the magnitude and distribution of particulate organic carbon (POC) and dissolved organic carbon (DOC). POC can be measured through sample filtration and land–lab analysis, but it would be preferable to obtain continuous profiles of POC at the resolution of a CTD. Transmissometers, instruments that measure beam attenuation, c, due to water and particles can be interfaced with a CTD. The portion of c due to particles, c_p, is known to be linearly related to particle concentration (Zaneveld, 1973; Bartz et al., 1978; Gardner et al., 1985; Bishop, 1986, 1999; Spinrad, 1986; Pak et al., 1988). Morel (1988) suggested there was a nearly linear relationship between particle light scattering and POC. During the JGOFS and other studies of the last two decades we also have found a very good linear correlation between in-situ c_p and POC concentration in sea water in the North Atlantic (Gardner et al., 1993), Equatorial Pacific (Gardner et al., 1995), Arabian Sea (Gundersen et al., 1998); Ross Sea (Richardson et al., 1999; Gardner et al., 2000b) the Pacific Southern Ocean (Gardner et al., 2000b; Mishonov and Gardner, 2003a), HOT (Mishonov and Gardner, 2003a) and the Gulf of Mexico (Richardson et al., 2003). Linear correlations also have been found by others in the Equatorial and North Pacific (e.g. Claustre et al., 1999; Bishop et al., 1999; Bishop, 1999).

In order to extend our POC coverage to a global scale, we worked with other scientists to interface our transmissometers on many WOCE cruises. We archived the raw data and the JGOFS Synthesis and Modeling Program provided an opportunity to process and synthesize the c_p data and convert these measurements to POC. Like the marine carbon dioxide survey, these global measurements have not been synoptic, but they were collected simultaneously with hydrographic data extending through the full water column.

For more than three decades great effort has been expended to "sea-truth" satellite ocean-color data via shipboard measurements to develop reliable algorithms to convert ocean color to chlorophyll-*a* concentrations (Morel and Prieur, 1977; Lewis et al., 1983; Morel, 1988; Morel and Berthon, 1989; Sathyendranath and Platt, 1997; Hooker and McClain, 2000; Morel and Maritorena, 2001; Sathyendranath et al., 2001). Those efforts are continually being refined, especially as new color sensors such as the sea-viewing wide field-of-view sensor (SeaWiFS) and moderate-resolution imaging spectroradiometer (MODIS) have become available (e.g. Aiken et al., 1998; Evans et al., 2000; Sathyendranath et al., 2000; Del Castillo et al., 2001; Shifrin, 2001). These efforts also are driven by the desire to understand biological processes and led to the development of algorithms to predict photosynthetic rates from chlorophyll concentration (Behrenfeld and Falkowski, 1997; Carr et al., 2006) and other parameters (Behrenfeld et al., 2005).

In Case I waters, where the chlorophyll concentration is high relative to the scattering coefficient (Morel and Prieur, 1977), most particles and POC originate from biological processes and there is a general covariation between chlorophyll-*a* and POC (Legendre and Michaud, 1999), though detailed differences have been examined (Kitchen and Zaneveld, 1990). The bulk carbon to chlorophyll-*a* ratio can vary by 10–40 fold (Morel, 1988; Chung et al., 1996) as proportions of phytoplankton, bacteria and detritus change (El-Sayed and Taguchi, 1981; Smith et al., 1996; Gundersen et al., 2001), and as the ratio of chlorophyll to phytoplankton carbon changes (e.g. Geider et al., 1998). Additionally, the intracellular distribution of chlorophyll within cells changes as a function of changing irradiance, temperature and nutrients (Behrenfeld and Boss, 2003). Since the mass of chlorophyll is small compared to bulk POC (1.5–4% for phytoplankton, Banse, 1977; Eppley et al., 1977, 1992), and because carbon to chlorophyll ratios change, it is extremely difficult to accurately estimate POC from chlorophyll concentrations measured either directly or by remote sensing. Efforts to measure or model complete carbon budgets (including export and remineralization) require more accurate data on POC concentration and distribution than can be derived from chlorophyll concentration. Thus, although there is general covariance between chlorophyll or POC concentrations and ocean color, it is desirable to develop algorithms to estimate POC concentrations directly from satellite ocean-color products. Stramski et al. (1999), Loisel et al. (2001), Mishonov et al., 2003b, and Behrenfeld et al. (2005) have proposed ways to accomplish that goal. In this paper we develop algorithms for POC concentrations from satellite data, examine seasonal differences and discuss possible interpretations of the constructed global maps.

2. Study areas

We have collected transmissometer data around the world since the early 1980's during JGOFS,

WOCE, and other programs such as the South Atlantic Ventilation Experiment (SAVE), North East Gulf of Mexico (NEGOM; shelf and slope), and Coastal Mixing and Optics (CMO; the shelf south of Martha's Vineyard, USA). Our data base includes c_p measurements from 51 cruises, and there are POC measurements from JGOFS and other cruises at 8 different regions of the world (see Fig. 1), including numerous cruises at the Hawaii Ocean Time-Series (HOT) and Bermuda Atlantic Time Series (BATS) sites. Temporal distribution of the transmissometer data is charted on the insert in Fig. 1.

3. Methods

3.1. Optical database

Our entire processed transmissometer data set consists of 7251 profiles and spans the period from 1983 to 2000. Our field measurements were made using one of 16 different 25-cm path-length SeaTech transmissometers interfaced with a CTD rosette.

The SeaTech transmissometer measures beam attenuation in the red spectral band ($\lambda = 660$ nm). Attenuation of the light beam across the transmissometer's 25-cm path-length (r) was obtained using the same procedure for all data making them comparable and uniform. In brief, the percent transmission (Tr) of light was measured and converted to beam attenuation coefficient (c) using the equation $c = -r^{-1}\ln(\mathrm{Tr})$. As explained by Pak et al. (1988), the beam attenuation coefficient can be described as the sum of attenuation due to particles (c_p), water (c_w), and colored dissolved organic matter (c_{CDOM}): $c = c_p + c_w + c_{CDOM}$. According to several studies, c_{CDOM} is small enough to be ignored in measurements at 660 nm in open waters (Bartz et al., 1978; Bricaud et al., 1981; Pak et al., 1988). Attenuation due to water c_w is essentially constant for this instrument at a value of 0.364 m^{-1}set at the factory.

The majority of original raw transmissometer data were acquired during both down- and up-casts of the CTD-rosette. The down-trace data usually are preferred because the optical sensor is less obstructed during descent. On the other hand, water bottles are nearly always tripped during the ascent, so it is essential to record transmissometer data at the time and depth of the bottle trip when water samples are used for c_p calibration. Having both down- and up-traces provides an opportunity to compare the two profiles to check for instrumental errors in the data and to use the up-trace data. Temperature hysteresis can cause slight differences between down and up traces, especially in areas where temperature gradients are large (Gardner

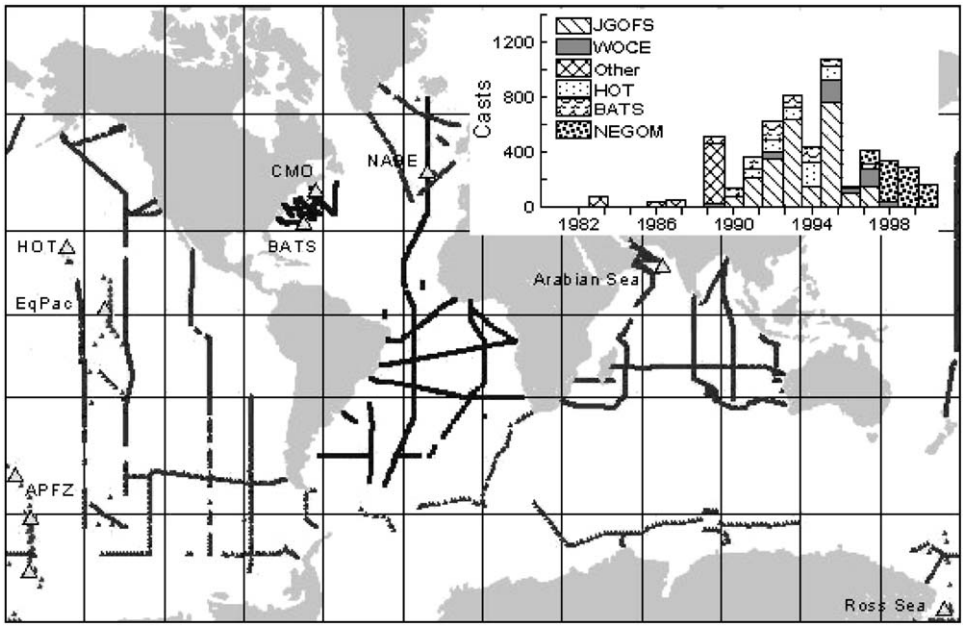

Fig. 1. Transmissometer stations and sites where POC was measured simultaneously (triangles). Insert: temporal distribution of the transmissometer data: # profiles per year.

et al., 1985; Bishop, 1986), but compared to the c_p signal in surface waters, this effect is small.

The data-processing procedure described below was applied uniformly to all data from WOCE and SAVE. HOT and BATS data were added for more temporal coverage but required more intensive processing, whereas JGOFS, NEGOM, and CMO data had been previously reduced and were in need of only minor corrections and final adjustments.

Raw-data files were processed with a customized software algorithm. Processing included (a) pressure checking and depth inversion filtering, (b) spike removal using two depth-dependent window filters and a c_p gradient check (single-point spikes were removed as they most likely represented individual large particles), (c) data averaging and reduction from the 30 Hz recording frequency to 2 db pressure intervals centered at even numbers, (d) application of the instrument's calibration data using pre-cruise, cruise and post-cruise calibration values, (e) removal of excessively noisy data, (f) profile smoothing by five-point running average, and (h) determination of profile minimum.

Our basic assumption was that deep-waters are highly stable and constant in terms of hydro-optical characteristics. The minimum c_p value, its depth and the station bottom depth were plotted for each profile on every cruise. This allowed detection of any cruise-long decay in the light-emitting diode intensity, dirty windows or instrumental offsets. The cruise trend evaluation used the profile minimum c_p values only at open-ocean, deep-water stations.

Profile adjustments were made by shifting the entire profile so that the profile's minimum c_p value in deepwater (from the zone deeper than 750 m and more than 750 m above the seafloor) was set equal to the cruise's minimum. Shallow-water stations were adjusted only by the mean offset in deep-water stations of each cruise. Gardner et al. (1985) used this method in modified ways during processing of the JGOFS transmissometer data and it seems widely applicable as long as data from deep water are available.

3.2. POC data

All of the POC data in this paper came from rosette water bottle samples. Bulk water samples include all organic particles filtered that were greater than the nominal pore size of filters used (typically GF/F filters; 0.7 μm), which includes heterotrophic bacteria, pico- nano- and microphytoplankton, microzooplankton, detritus, and may occasionally include some small mesozooplankton (Legendre and Michaud, 1999; Liu et al., 2005). Additionally there can be DOM absorbed on the filter (Menzel, 1967; Moran et al., 1999). POC sampling and processing were performed for all the data by several different investigators following a standard protocol (Knap et al., 1994, http://www.uib.no/jgofs/Publications/Report_Series/JGOFS_19.pdf). In general, during the cruises water collected at specific depths was drawn from Niskin bottles and filtered at low vacuum (0.25 atm) through a funnel setup onto 25-mm glass fiber filters (GF/F). None of the samples were pre-filtered to remove macrozooplankton other than the HOT samples (http://hahana.soest.hawaii.edu/hot/protocols/chap10.html). Filters were dried at 60 °C for eight hours, wrapped with pre-combusted aluminum foil and stored in a sealed plastic bag. Onshore, filters were acidified to remove carbonates and analyzed by combustion with elemental analyzers according to JGOFS protocols (Knap et al., 1994; JGOFS, 1996), most often at the Bermuda Biological Research Station. The same methods were used to analyze some samples at Horn Point Marine Laboratory and the Virginia Institute of Marine Science. Filter blanks were pre-combusted filters taken to the field, but no filtered water was passed through the blanks. Adsorption of DOC and colloidal organic carbon onto filters (Moran et al., 1999; Gardner et al., 2003a), most notably at low concentrations ($<4\,\mu M$), could have introduced a positive bias in the measured POC values.

3.3. Beam c_p and POC database

Some POC data (Fig. 2) were obtained from geographically small locations: North Atlantic (NABE; Gardner et al., 1993), Equatorial Pacific (EqPac; Gardner et al., 1995; Walsh et al., 1997), Ross Sea (Gardner et al., 2000a), shelf south of Cape Cod, Massachusetts (CMO; Gardner et al., 2001) and NEGOM area (Bernal, 2001; Richardson et al., 2003) (see triangles on Fig. 1). In other areas the geographic coverage was basin-wide: Arabian Sea (Gundersen et al., 1998) and Antarctic Polar Front Zone (APFZ; Gardner et al., 1999). BATS (Steinberg et al., 2001; Mishonov and Gardner, 2003a) and HOT (Hebel and Karl, 2001; Mishonov and Gardner, 2003a) POC data also were added.

The simultaneously collected c_p and POC data were used to assess the c_p:POC relationship. The total of all simultaneous c_p:POC data available

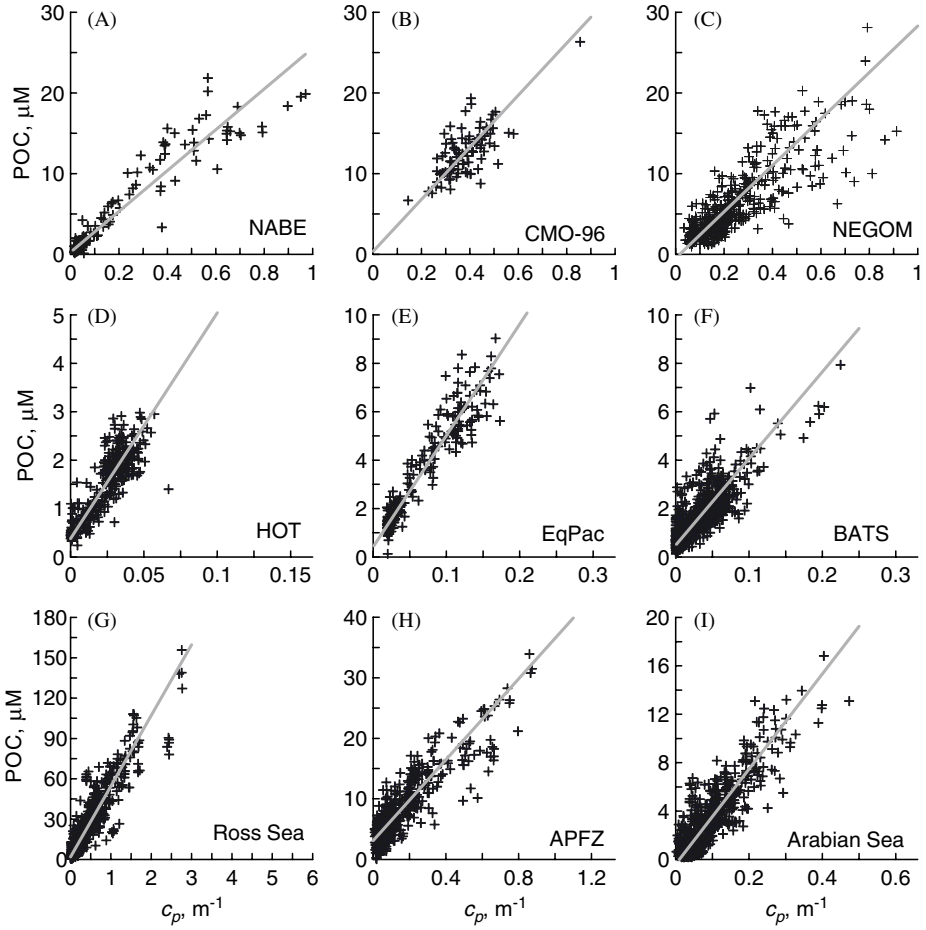

Fig. 2. Regressions between POC and Beam c_p acquired in different regions: (A) North Atlantic Bloom Experiment (NABE) modified from Gardner et al. (1993). (B) Coastal Optics and Mixing experiment, 1996 (CMO-96) modified from Gardner et al. (2001). (C) North-East Gulf of Mexico (NEGOM) modified from Richardson et al. (2003). (D) Hawaii Time Series (HOT) corrected data from HOT archives, modified from Mishonov and Gardner (2003a). (E) Equatorial Pacific (EqPac) JGOFS, R.V. *Th. Thomson* cruise TT012. Beam c_p from Gardner et al. (1995), Chung et al. (1996, 1998); POC from JGOFS data base. (F) Bermuda Atlantic Time Series (BATS), corrected data from BATS archives, modified from Mishonov and Gardner (2003a). (G) Ross Sea—AESOPS, R.V. *N.B. Palmer* cruises NBP 96-3, NBP 96-8, NBP 97-1, NBP 97-3, NBP 97-8, & NBP 98-2. Modified from Gardner et al. (2000a). (H) Antarctic Polar Front Zone (APFZ), R.V. *R. Revelle* cruises KIWI-6, 7, 8, & 9. Modified from Morrison et al. (2001), Gardner et al. (2000b). (I) Arabian Sea—JGOFS, R.V. *Th. Thomson* cruises TN043, TN045, TN049 and TN054. Modified from Gundersen et al. (1998).

from JGOFS process studies and from our other projects consists of 2858 data pairs. In order to increase temporal and spatial coverage we added c_p:POC data collected at HOT (306 data pairs) and BATS (855 data pairs). The c_p data collected at these two sites have been re-analyzed and corrected (Mishonov and Gardner, 2003a). We also utilized seasonal data from the NEGOM project collected during nine cruises over 3 years (440 data pairs, Bernal, 2001; Richardson et al., 2003), bringing the total data pool to 4456 pairs. All data were combined into a single composite plot (Fig. 3). Correlation statistics are in Table 1.

It should be noted that POC is calculated using c_p at 660 nm, and that most of the light attenuation and scattering are dominated by the 0.5–20 µm fraction of the particle size spectra, with a peak sensitivity around 1–2 µm (Stramski and Kiefer, 1991; Chung et al., 1996, 1998; Boss et al., 2001). This is the size fraction in which phytoplankton contribution is greatest. The dominant contribution to POC (in open-ocean waters) has been demonstrated on multiple occasions to be phytoplankton (e.g., Eppley et al., 1992; DuRand and Olson, 1996; Gundersen et al., 2001; Green et al., 2003; Green and Sosik, 2004).

c_p and POC sections and maps compiled from all processed data have been generated and can be viewed on our project web-site at http://oceanography.tamu.edu/~pdgroup/SMP_prj/DataDir/SMP-data.html (data locations shown in Fig. 1). c_p data merged with temperature, salinity and oxygen data and stored in Ocean Data View (Schlitzer, 2003) software format also can be downloaded.

3.4. Satellite data

3.4.1. SeaWiFS versus c_p regression

To compare in-situ data with remotely sensed optical parameters, values of c_p were averaged from vertical profiles down to one attenuation depth of the ocean, assuming that is the maximum depth from which a remotely sensed signal is radiated. One attenuation depth was calculated based on SeaWiFS-derived diffuse attenuation coefficient (K_{490}) data using the formula $z = 1/K_{490}$ (Gordon and McCluney, 1975). This depth varied from 9 to 29 m in the APFZ area, and from 1 to 30 m in the NEGOM and SAVE areas. The APFZ and NEGOM data have synchronous satellite and in-situ data. The SAVE data in the Mishonov et al. (2003b) paper uses satellite data from the same seasons, but from later years since ocean-color satellites were not operating during the SAVE program.

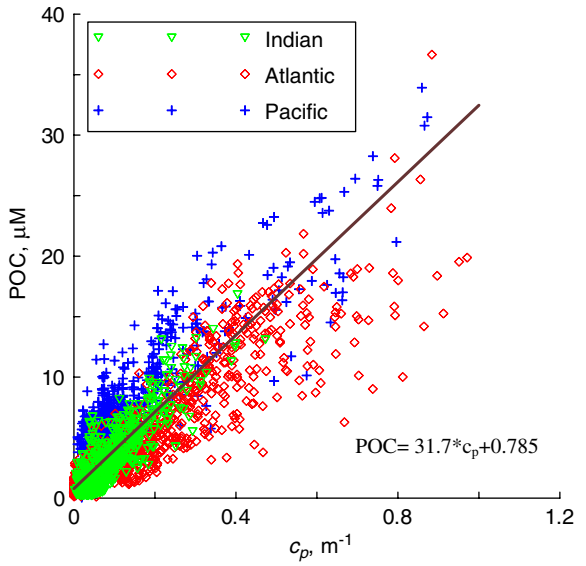

Fig. 3. Global POC—Beam c_p regression calculated on all available data collected in Indian (∇), Atlantic (◇) and Pacific (+) oceans. See Table 1, "All data" for regression parameters.

Data for K_{490}, normalized water leaving radiance at 555 nm $L_{WN}(555)$, chlorophyll concentration (CHL) and integral chlorophyll ($I_{CK} = CHL/K_{490}$), i.e. chlorophyll integrated in one attenuation depth (Campbell et al., 1995), were extracted from the SeaWiFS data archives (http://daac.gsfc.nasa.gov/data/datapool/SEAWIFS/index.html). To provide better satellite data coverage in a cloudy area such as the APFZ (and NEGOM in some seasons) we used 8-day SeaWiFS composites (Level 3, 9 × 9 km, i.e. 1 × 1 pixels, Reprocessing 4 data). The total dataset (Table 2) consists of 580 data points: 140 for APFZ and 440 for NEGOM. Calculations from the 330 data point from SAVE (Mishonov et al., 2003b) also are listed.

3.4.2. APFZ area

For comparison with c_p, satellite data were averaged over the time-scale appropriate to each cruise (one to three 8-day mosaics). Expedition KIWI cruises 6 and 8 covered a small geographical area due to ice coverage and a focus on the Polar Front Zone. For KIWI-Process cruises (7 and 9)

Table 1
Parameters of the Model II linear regression for different regions of the World Ocean: beam attenuation due to particles (c_p, 1/m) vs. POC (μM) concentration

MOD II params.	Regions									
	NABE	CMO-96	NEGoM	HOT corr.	EqPac	BATS corr.	Ross Sea	APFZ	Arabian Sea	All data (no RS)[a]
Slope	25.3	32.2	27.6	46.6	46.0	35.8	52.6	33.5	39.3	31.7
Intercept	0.276	0.374	−0.457	0.381	0.420	0.494	1.902	3.064	−0.388	0.785
SD slope	0.610	2.399	0.737	1.439	0.975	0.709	0.592	0.609	0.707	0.275
SD intercept	0.178	0.943	0.218	0.042	0.078	0.032	0.304	0.125	0.078	0.048
n	165	88	440	305	224	855	994	659	726	3462
R^2	0.904	0.513	0.685	0.710	0.899	0.664	0.874	0.781	0.766	0.739

[a]No Ross Sea data used in global fit.

Table 2
Regression between synchronous c_p and SeaWiFS data products observed in Northeast Gulf of Mexico (NEGoM, 440 data points) and Antarctic Polar Front Zone (APFZ, 140 data points)

Parameters	SeaWiFS data products												
	CHL			K_{490}				$L_{WN}(555)$			IC_K		
Region	NE GoM	APFZ	SAVE	NE GoM	APFZ	Combined	SAVE	NE GoM	APFZ	SAVE	NE GoM	APFZ	SAVE
Slope	0.567	1.022	0.537	1.119	1.897	1.124	1.476	1.388	1.969	2.502	1.123	2.156	0.810
Intercept	−1.228	−0.306	−1.013	1.254	3.856	1.361	2.560	−0.636	−0.186	0.601	−3.730	−5.068	−3.018
RMS	0.131	0.090	0.062	0.130	0.107	0.166	0.040	0.249	0.090	0.048	0.047	0.080	0.084
R^2	0.714	0.805	0.801	0.716	0.768	0.638	0.871	0.455	0.804	0.847	0.850	0.826	0.730

Non-synchronous regression parameters from the South Atlantic Ventilation Experiment (SAVE, 330 data points adopted from Mishonov et al., 2003) are shown for comparison. SAVE c_p data are compared with climatological SeaWiFS data from later, non-overlapping years. Equation: $c_p = \mathrm{EXP}(\mathrm{Slope} \times \mathrm{LN}(\mathrm{Product}) + \mathrm{Intercept})$. Combined—combined regression using APFZ and NEGOM datasets.

satellite data were averaged over the period of southbound and northbound transects of each of the cruises. Field data on c_p and POC were collected during different stages of the plankton bloom that developed in the vicinity of the Polar Front (~61°S) over a 5-month period. The dynamic character of the optical field in the vicinity of the Polar Front is illustrated in Fig. 4, where mosaics (A)–(F) show the variability of the K_{490} field during successive 2–3 week periods (sampling station positions also are marked).

3.4.3. NEGOM area

All nine cruises were 10–11 days long, so single eight-day SeaWiFS mosaics falling into that timeframe were compared with the field data, providing good data coverage with a relatively small area obstructed by clouds. The NEGOM program covered different seasons (spring, summer, fall) for 3 years, spanning different hydrologic conditions. Variations in the Mississippi River outflow, different locations of the loop current, and seasonal phytoplankton blooms resulted in significant variability of c_p and POC in the upper water column. This variability is also well represented in the K_{490} field shown as a background in Fig. 5.

3.4.4. Temporal changes in POC from satellite color products

Although biogeochemical process studies from ships in a single location provide the opportunity to monitor changes over time for a body of water, they are obviously limited in spatial coverage, as well as time (length of a cruise). Satellites provide far greater synoptic spatial coverage than is possible with shipboard, moored, or profiling measurements, so it is highly desirable to develop reliable algorithms for quantifying POC from satellite ocean color. It is necessary to sea-truth algorithms in as many regions and seasons as possible in order to assure their reliability. Basin-wide hydrographic/carbon programs, like the CLImate VARiability (CLIVAR) Repeat Hydrography program, provide an unprecedented opportunity to simultaneously measure all components of the carbon system in a variety of oceanic conditions at a time when satellite ocean color data are available. Once algorithms are refined, they will provide a new tool to quantify POC in surface waters at any time and location that ocean-color data are available. With simultaneous data on POC and chlorophyll concentrations we can make time-series measurements to follow the evolution of an event to quantify changes in concentration and percentage of these two important components. Time series of chlorophyll concentration already exist for some areas (e.g., Kahru et al., 2004). Time series data on concentrations of both chlorophyll and POC should provide even better constraints on the output of biogeochemical models than chlorophyll alone.

4. Results

4.1. c_p:POC regressions by region

The large data set of c_p and POC allows us to assess relationships between c_p and POC in different regions over different seasons. In Fig. 2 all data,

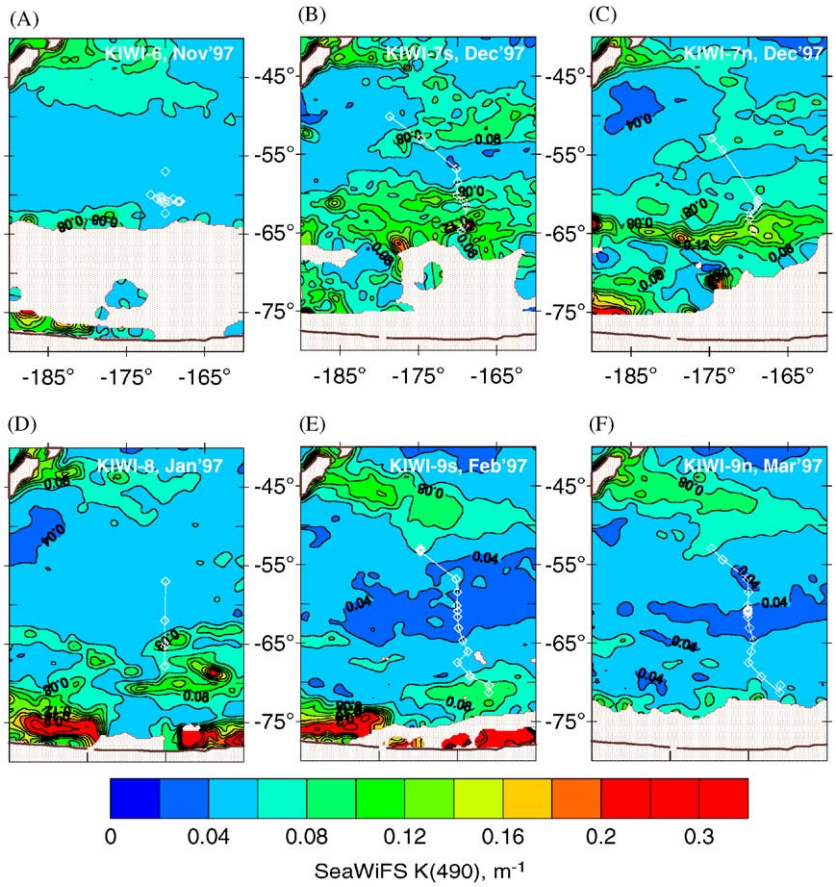

Fig. 4. SeaWiFS diffuse attenuation coefficient at 490-nm data averaged over cruise time-span for different KIWI cruises/legs in Antarctic Polar Front Zone (APFZ) area. Dots along cruise tracks denote station positions. See text for details.

collected under a wide variety of physical and geographical conditions, are presented as c_p versus POC scatter plots. For comparability plots are shown on the same relative X– Y scale but with different ranges so that regression slopes can be visually compared. Since beam c_p is a function of particle size, shape and index of refraction (Zaneveld, 1973; Twardowski et al., 2001), it is reasonable to expect the beam c_p to POC relation to vary regionally and temporally during the cycle of a bloom and spatially as regimes with different community structures are encountered with plankton of different composition (organic, siliceous, carbonate) and size spectra.

Based on more than 7000 c_p profiles, there is little variability in structure of the c_p profiles below 200–300 m except near some continental margins and close to the sea floor. In regions of resuspended sediments, beam c_p should be regressed against total particulate matter concentration (PMC), which still yields a linear correlation, but with a different slope (Spinrad et al., 1983; Gardner et al., 1985, 2000b; Gardner, 1989; Gundersen et al., 1998). Analysis of the near-bottom beam attenuation data is not in the scope of this work.

Slopes of the Model II c_p:POC linear regressions for regional datasets appear to be relatively close, especially within a given oceanic region (Fig. 2). Parameters of these regressions are shown in Table 1. The major exception is the Ross Sea regression—its slope is twice that for NABE or NEGOM. The larger slope might be due to a difference in the physiology and composition of plankton produced in this regional ecosystem during the intensive phytoplankton blooms (Smith et al., 2000). While we have documented some seasonal and spatial fluctuations in the c_p:POC relationship (e.g., Gundersen et al., 1998), the year-round data collected in the Arabian Sea, HOT, and BATS show the annual variations to be small. Therefore, for this large-scale analysis we have

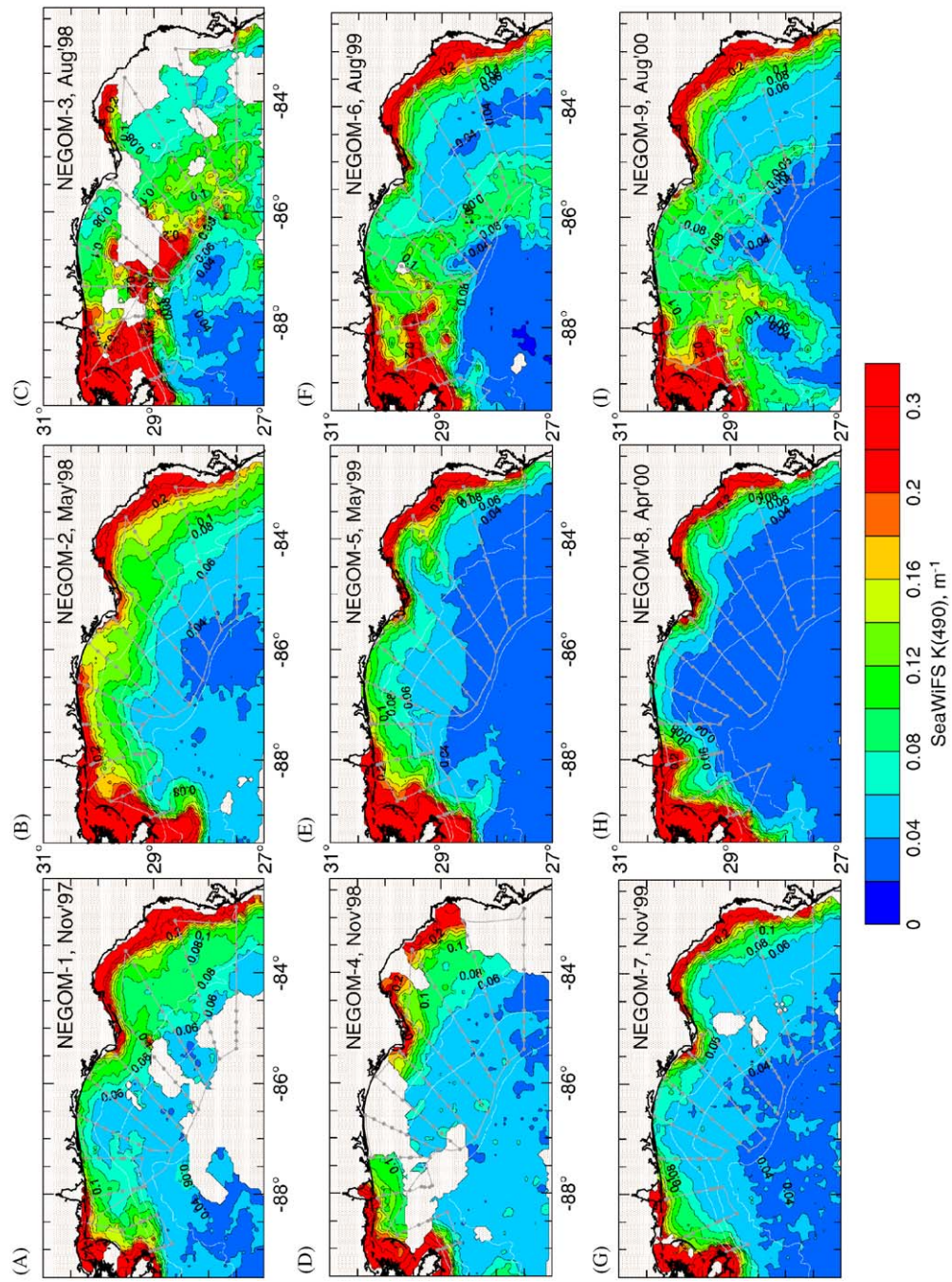

Fig. 5. SeaWiFS diffuse attenuation coefficient at 490-nm data averaged over cruise time-span for different NEGOM cruises in the Northeast Gulf of Mexico. Dots along cruise tracks denote station positions. See text for details.

combined all data (excluding the Ross Sea) to produce a single global c_p:POC ratio (Fig. 3). Bishop (1999) advocated this approach, although some regional and seasonal variations obviously exist.

The resulting dataset consists of 3462 data pairs (excluding 994 Ross Sea pairs), which were assembled into one data pool and a general regression between c_p and POC was constructed. Fig. 3 shows the global property–property plot with the Model II regression line (parameters of this regression are shown in the last column of the Table 1). Obviously a general combined regression is a compromise: from Fig. 3 it is clear that in the Pacific this regression will underestimate values of POC (blue crosses), while in the Atlantic POC values will be slightly overestimated (red diamonds). For the Indian Ocean this regression is a good fit (green triangles), although all Indian Ocean data were collected in the Arabian Sea.

4.2. SeaWiFS products versus c_p regression

Mishonov et al. (2003b) used shipboard c_p data collected in the South Atlantic in 1987–1989 regressed against four SeaWiFS data products seasonally averaged for 1997–2002 because no synchronous satellite data were available. Despite the decade gap between datasets, there was a reasonable correlation between c_p and $L_{WN}(555)$ ($r = 0.882$) and K_{490} ($r = 0.800$) using an exponential regression when Case II waters were eliminated.

In this paper, we used only synchronous datasets of c_p, POC, and SeaWiFS-derived ocean-color products collected during the APFZ and NEGOM programs to derive empirical algorithms. In addition to $L_{WN}(555)$ and K_{490}, comparisons were made with CHL and $I_{CK} = \mathrm{CHL}/K_{490}$. The four SeaWiFS data products were plotted versus c_p averaged over one attenuation depth (Fig. 6), and several types of regression fits were calculated and evaluated for all data products. Two parameters, K_{490} and $L_{WN}(555)$ produced very good relationships in both regions, but K_{490} produced somewhat less scatter and a higher overall correlation than $L_{WN}(555)$ and was selected for further use. The resulting equation is

$$c_p = \mathrm{EXP}(1.124 \times LN(K_{490}) + 1.361).$$

The comparable relationship for SAVE data is

$$c_p = \mathrm{EXP}(1.476 \times LN(K_{490}) + 2.560).$$

Parameters of each regression are presented in Table 2. Maps were made and evaluated independently using both K_{490} and $L_{WN}(555)$, but the maps and figures in this paper are only from K_{490} data using synchronous APFZ and NEGOM data.

It is encouraging that regressions based on in-situ and seasonally averaged SeaWiFS data collected 10 years later match well with regressions based on synchronously collected data for two of the parameters tested (Fig. 6). This is most likely due to the fact that the 5-month average of K_{490} and $L_{WN}(555)$ done by Mishonov et al. (2003b) showed that about 80% of the area of this averaged data had a standard deviation of less that 20% during a 5-year period.

4.3. Global POC distribution from SeaWiFS products

To produce global seasonal maps of POC, SeaWiFS K_{490} data were averaged over a 5-year period (1997–2002) for summer (May–August) and winter (December–March) seasons (maps not shown). Using the c_p:K_{490} regression (Table 2, Fig. 6(B)) the K_{490} field was converted to a global map of c_p (not shown). Finally, the c_p field was converted to POC for summer (Fig. 7(B)) and winter (Fig. 8(B)) seasons using the global c_p:POC regression (Table 1, Fig. 3). POC was recalculated in units of $\mathrm{mg\,m^{-3}}$ rather than $\mu\mathrm{M\,m^{-3}}$ for consistency with SeaWiFS-derived chlorophyll concentration data.

4.4. POC predicted versus POC measured

In order to estimate the reliability of the global K_{490}:c_p:POC transformation we plotted the predicted POC values (from K_{490}:c_p:POC) for APFZ and NEGOM against the synchronously measured POC values from filters (Fig. 9). This was done using both the global regression and the regional regression for both areas. For NEGOM the fit is better overall than for APFZ, but the values are generally overestimated. This is most notable at low concentrations where measured values are as low as 2 μM, while the minimum predicted values are about 3 μM. In the APFZ, minimum measured and predicted values are both about 3 μM, but the higher predicted POC values are underestimated significantly by the global regression, which is also a known problem with chlorophyll algorithms for high latitudes (Kahru and Mitchell, 1999; Stramska et al., 2003). This could be due partially to the effects of low solar zenith angle on remotely sensed signals for high-latitude areas. Another reason could be a statistical

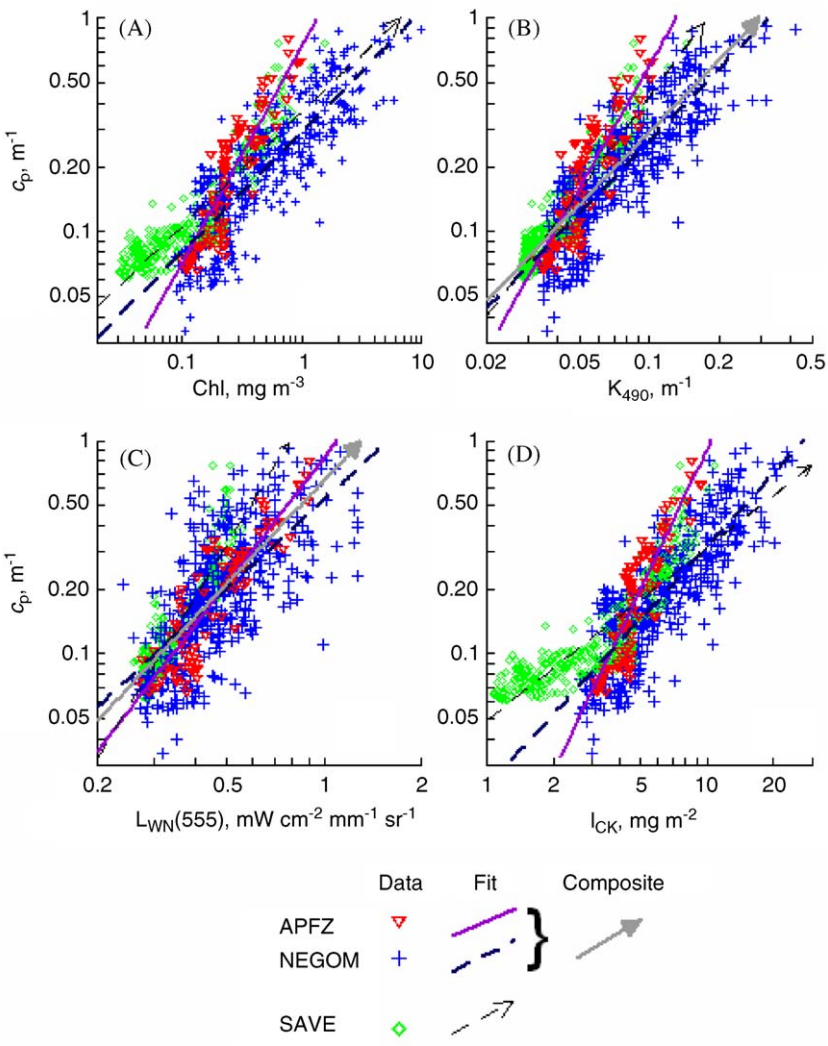

Fig. 6. Regressions between beam c_p and four SeaWiFS products calculated with simultaneously collected data: APFZ (∇) and NEGOM (+), modified from Richardson et al. (2003); and seasonally averaged data: SAVE (◇), modified from Mishonov et al. (2003b): (A) SeaWiFS chlorophyll, CHL; (B) SeaWiFS diffuse attenuation coefficient at 490 nm, K_{490}; (C) SeaWiFS normalized water-leaving radiance at 555 nm, $L_{WN}(555)$; (D) SeaWiFS chlorophyll integrated over one attenuation depth, I_{CK}. The regression used for global maps in Figs. 8 and 9 is the solid gray line in (B), which is a composite of the c_p:K_{490} data collected at APFZ and NEGOM.

influence since there are nearly three times as many NEGOM data points as APFZ points used for the regression calculation and the difference in slopes (Table 2) reduce the predicted APFZ POC values—this is an expected drawback of using a global algorithm. This issue could possibly be improved by incorporating more data or switching to regional regressions. The regional regressions give better results, decreasing the values in NEGOM and increasing the values in APFZ, but using regional algorithms creates discontinuities at the regional boundaries. Using $L_{WN}(555)$ instead of K_{490} provided higher maximum values of POC, but the scatter was greater in the correlation with POC.

Comparisons of our predicted POC values at low concentrations also can be made at HOT and BATS. Hebel and Karl (2001) plotted POC data from 1989 to 1997 indicating that surface values were between 2 and 4 μM. Our predicted average values at HOT were 3.5 μM for both summer and winter. Archived values at BATS are similar, and our predicted average values were 3.6 μM for summer and 4.5 for winter. The JGOFS EqPac POC data at 140°W from 12°S to 12°N yielded

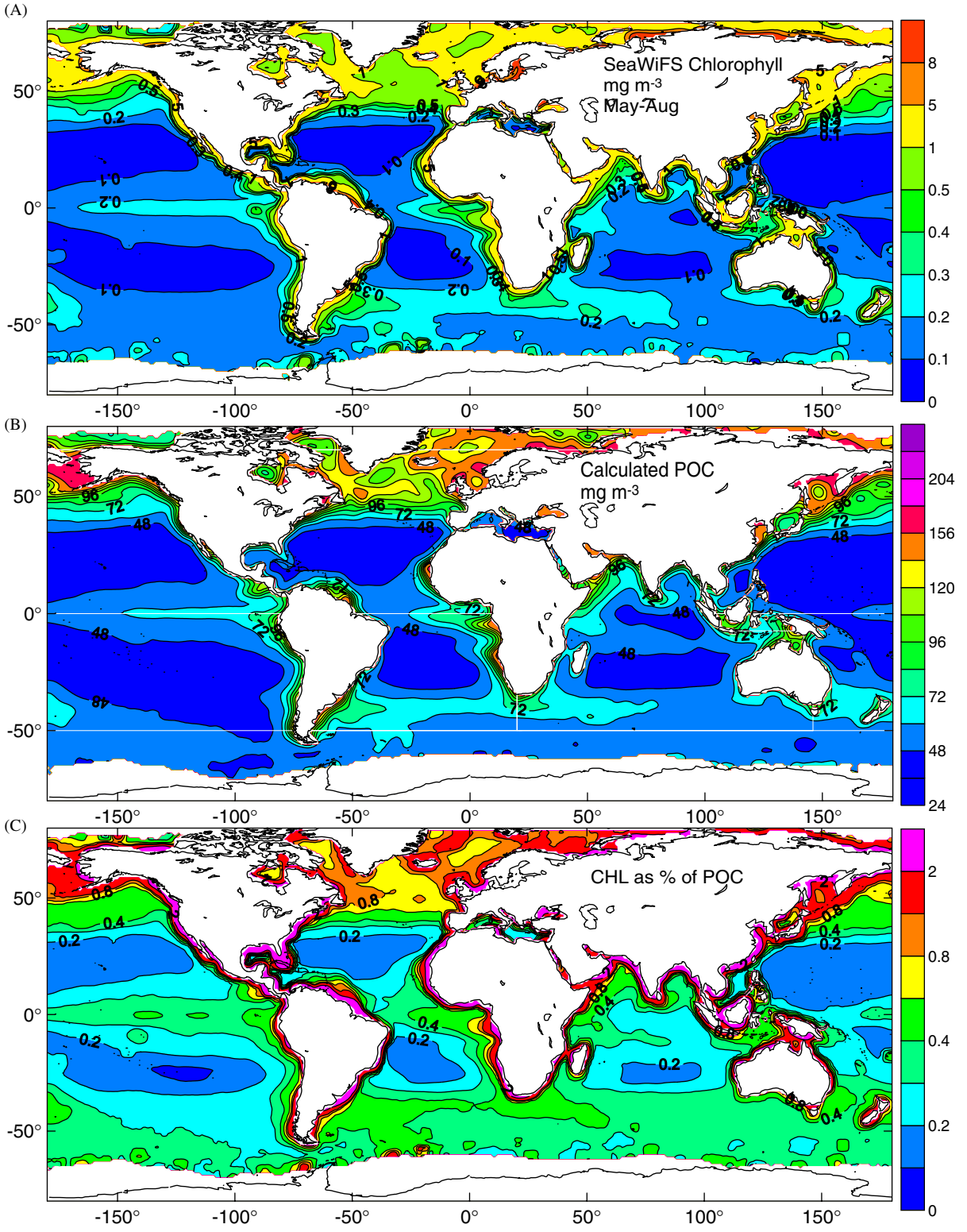

Fig. 7. Global distribution for summer season (1997–2002, May–August, 20 months) of: (A) SeaWiFS CHL (mg m^{-3}, level 3, reprocessing 4 data); (B) average POC (mg m^{-3}) over one attenuation depth calculated from K_{490}:c_p:POC; (C) CHL as a % of POC. White lines in (B) mark boundaries separating ocean basins as used by Behrenfeld and Falkowski (1997) and in Table 3.

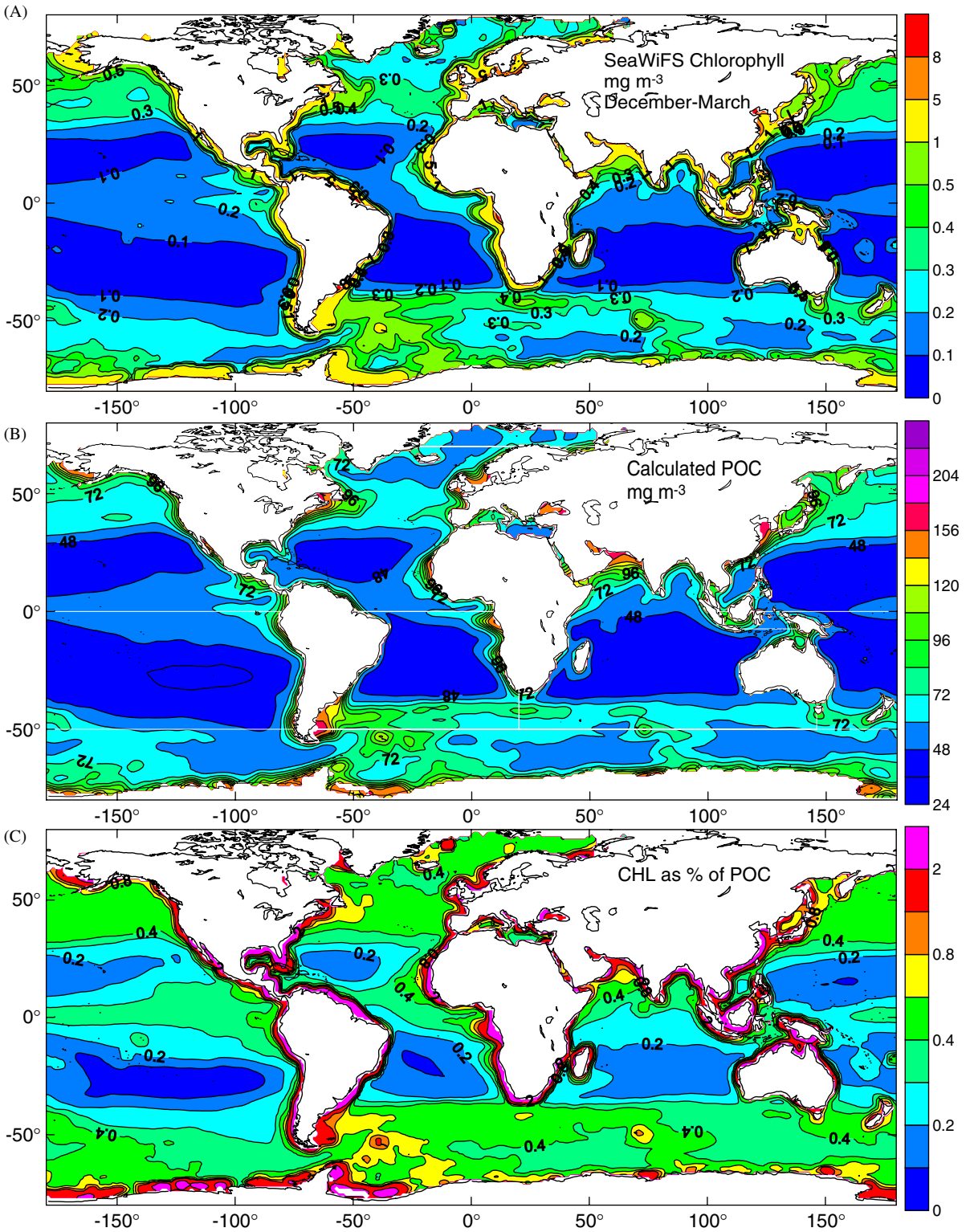

Fig. 8. Global distribution for winter season (1997–2002, December–March, 20 months) of: (A) SeaWiFS CHL (mg m^{-3}, level 3, reprocessing 4 data); (B) average POC (mg m^{-3}) over one attenuation depth calculated from K_{490}:c_p:POC; (C) CHL as a % of POC. White lines in (B) mark boundaries separating ocean basins as used by Behrenfeld and Falkowski (1997) and in Table 3.

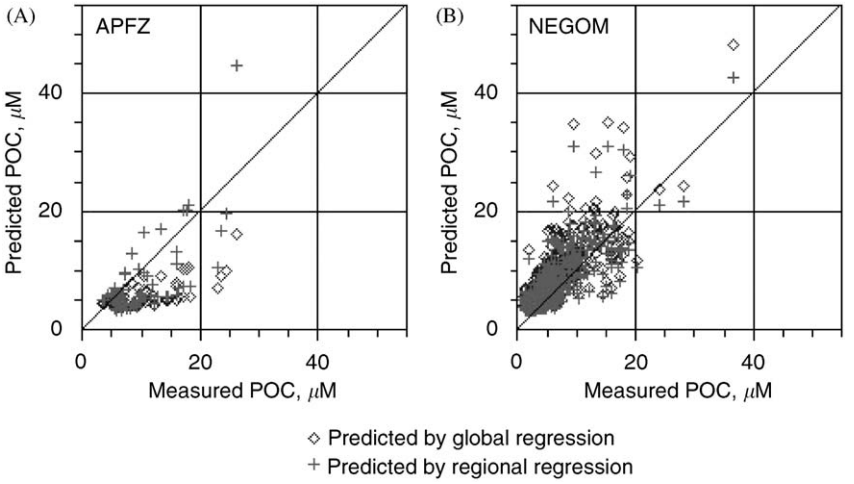

Fig. 9. Predicted POC versus measured POC concentration (μM) for (A) APFZ area; (B) NEGOM area.

bottle POC values between 3 and 5 μM, which is comparable to values in Figs. 7 and 8. The measured and predicted values of POC may both be 1–2 μM high, because both are based on bottle POC values, which may be 1–2 μM high due to DOC adsorption on the filters (Moran et al., 1999; Gardner et al., 2003a).

4.5. POC, c_p and chlorophyll

For comparison of POC and c_p with chlorophyll we compiled seasonal 5-year (1997–2002) averaged global maps from SeaWiFS CHL data for the same period (Figs. 7(A) and 8(A)). A bulk carbon:chlorophyll ratio could be obtained by simple division of the data in Figs. 7 and 8(A and B), but this could be confused with the typical carbon:chlorophyll ratios used in analyzing phytoplankton (Geider et al., 1998). Mishonov et al. (2003b) mapped CHL as a percent of POC ((CHL:POC)100) to look at spatial variations in the carbon:chlorophyll relationship, and we have made similar maps here (Figs. 7 (C) and 8(C)). Behrenfeld and Boss (2003) argued that c_p is a better proxy for phytoplankton biomass than for POC. They suggested a parameter of c_p normalized to chlorophyll concentration, c_p:CHL, or c_p^* with units of m^2 $mgCHL^{-1}$. Following this suggestion we have taken the c_p fields used to derive Figs. 7(B) and 8(B) and divided them by the matching spatial chlorophyll data (Figs. 7(A) and 8(A)) to produce summer and winter maps of c_p^* (Fig. 10). This relationship bypasses any conversion to POC.

5. Discussion

A major goal of the oceanographic community is to develop regional and global mass balances for carbon in order to understand the role of the ocean as a source and sink for atmospheric CO_2 because of its impact on earth's climate. To better understand and predict cycling of carbon and associated elements in the ocean, we must understand better the distribution and cycling of a very mobile component of the carbon cycle—particulate organic carbon (POC). CO_2 and dissolved organic carbon (DOC) in the surface ocean are converted to POC through biological processes. While CO_2 and DOC move with the water, POC can settle through the water, across isopycnals, scavenging or aggregating other particles and transporting carbon and associated elements to deeper waters where they enter the sediments or, more likely, are remineralized. Because carbon is the primary "currency" used in energy budgets of biogeochemical processes in the ocean, it is essential to quantify local and global carbon abundance. Although particulate organic carbon is a small component of the total carbon budget, it is a dominant component of primary production, which creates particles that can sink and transport carbon to deep waters. Deuser et al. (1983) also demonstrated that the flux of non-biogenic particles from the sea surface is controlled by biological processes related to POC flux. As ocean observing systems develop, we need data on c_p:POC and other bio-optical relationships in more

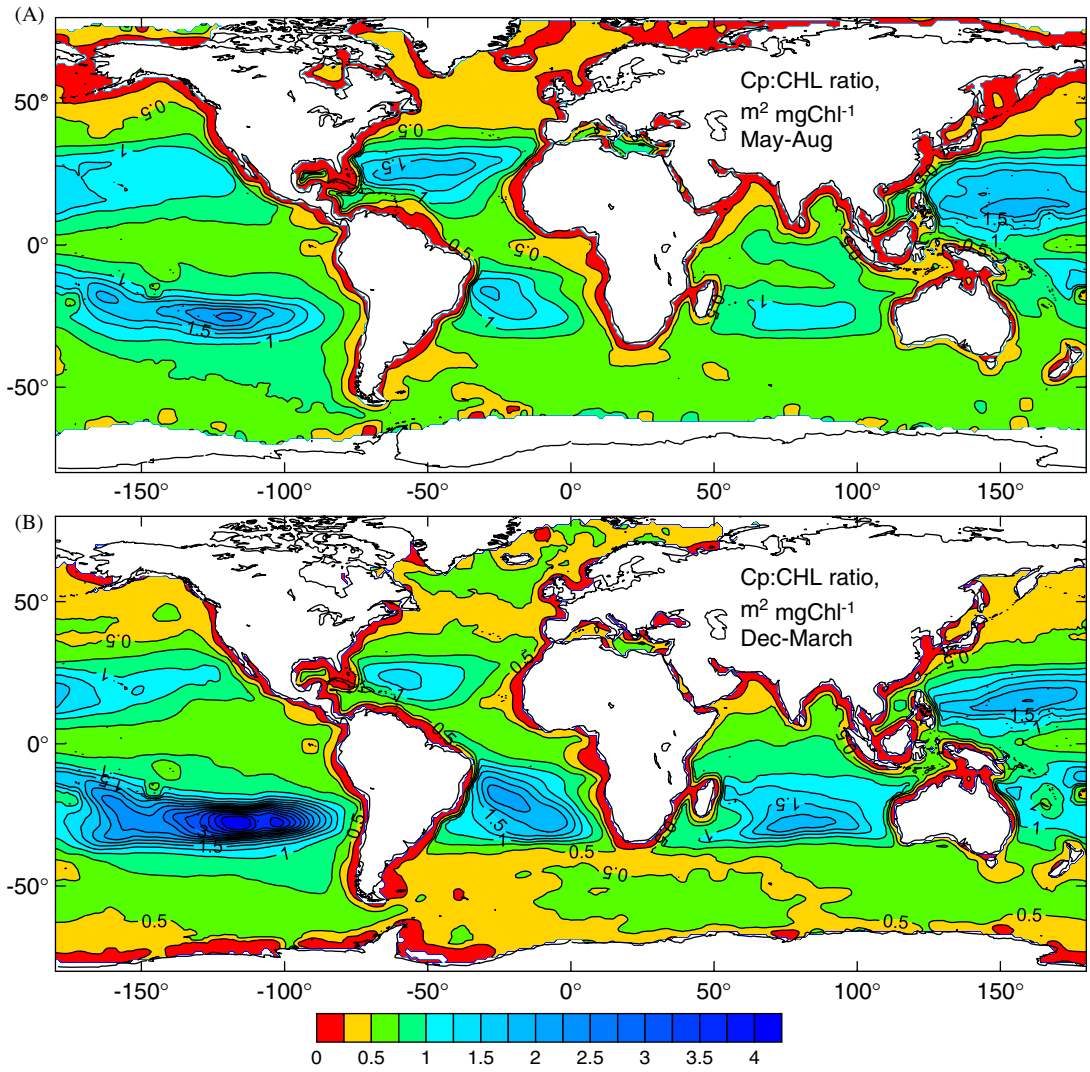

Fig. 10. Global distribution for (A) summer and (B) winter season (1997–2002, December–March, 20 months) of c_p:CHL, m^2 mgCHL^{-1} (c_p^* of Behrenfeld and Boss, 2003).

places during different seasons to determine the temporal and spatial variability of these parameters so they can be applied more confidently to the data collected from ships, moored and autonomous sensors. The utility and importance of this capability was elegantly demonstrated in the North and South Pacific by Bishop et al. (2002, 2004).

To improve biogeochemical and ecosystem models (e.g., Geider et al., 1998; Christian et al., 2002; Schlitzer, 2002; Hood et al., 2003; Jackson and Burd, 2002), it is necessary to obtain more accurate POC data than can be obtained from estimates based on chlorophyll concentrations (Legendre and Michaud, 1999). In this paper we have presented a new empirical algorithm to estimate POC concentrations from ocean-color products. As a demonstration of its application we averaged all ocean data over 5 years (1997–2002) for two seasons (Figs. 7 and 8; May–August and December–March). Such averaging results in the smoothing of small-scale details and interannual variability, but we chose this path to examine large-scale trends in this summary of global distributions.

Regarding the distribution of chlorophyll as a percentage of POC (Figs. 7(C) and 8(C)), chlorophyll percentage is susceptible both to changes of pigment/carbon within the phytoplankton (Banse, 1977; Eppley et al., 1977, 1992; Geider et al., 1998)

and changes in composition of the different carbon pools relative to phytoplankton pigment (El-Sayed and Taguchi, 1981; Smith et al., 1996; Gundersen et al., 2001). The % chlorophyll contours of 1.0 and 0.2 are equivalent to C:CHL ratios of 100 and 500, respectively.

Behrenfeld and Boss (2003) argued that c_p^* is an optical index of phytoplankton physiology in surface waters. They cited several observations where changes in c_p^* with depth were consistent with expected changes in photoacclimation, or changes in growth irradiance, which cause changes in intracellular chlorophyll concentrations that have been observed as a function of depth (Kitchen and Zaneveld, 1990; Mitchell and Kiefer, 1988; Mitchell and Holm-Hansen, 1991; Fennel and Boss, 2003). Behrenfeld and Boss (2003) also argued that if the c_p^* and photoacclimation relationship holds in the vertical dimension it also could hold in the horizontal and temporal dimensions as well. They noted that c_p is largely insensitive to changes in intracellular chlorophyll concentration, so changes in c_p^* could be an indication of changes in the physiological state of phytoplankton cells due to changes in irradiation, nutrients and temperature. Therefore, changes in c_p^* could provide information about spatial and temporal variability in the combined effects of cellular chlorophyll, incident light, and growth rate of the plankton at that location. Using existing data from HOT, BATS, NABE and EqPac, they found a first-order correlation between c_p^* and chlorophyll-normalized photosynthetic rate, P_{opt}^b. Behrenfeld et al. (2005) went on to show that c_p^* could be used with other parameters not only to look at phytoplankton physiology from space, but also to calculate carbon-based net primary production.

5.1. Regional observations

Mishonov et al. (2003b) created maps of POC concentration for the North and South Atlantic using satellite data averaged over just 1 month, yielding much finer detail than is seen in our 5-year averages over four summer or winter months (Figs. 7 and 8). Weekly or daily maps would reveal even greater detail, but the likelihood of complete aerial coverage decreases because of cloud cover. In examining these global maps each reader is likely to focus on geographic regions of their interest to look for specific features; we comment here on some general observations. Note that scales for CHL and POC are linear at the low end, yet this lower range covers approximately 80–90% of the ocean area. Scales are non-linear at the upper end and were chosen to best portray features in the areas of high gradients, which cover $<10\%$ of the ocean. The % CHL scale in Figs. 7(C) and 8(C) is linear only to 0.4%, which covers the majority of the ocean. Areas with $>2\%$ CHL are rare outside of coastal regions. The c_p^* scale in Fig. 10 is linear only in the lower range, with low values indicating a greater abundance of chlorophyll per phytoplankton cell than at large values of c_p^*. Thus, the shelf areas and regions of higher productivity have lower c_p^* values than the oligotrophic gyres. Both our c_p and CHL maps are parameters derived from ocean-color products, but they still match quite well with the in-situ measurements of c_p and chlorophyll that Behrenfeld and Boss (2003) used in their analysis of c_p^*. For instance c_p^* ranged between 0.14 and 1.6 at HOT over several years, 0.08–1.42 at BATS over several years, 0.25–0.84 at NABE over 2 months, and 0.22–0.7 at EqPac during parts of a year. They did not provide data from any shelf regions. The 5-year averages of our maps do not allow one to visualize temporal variations, but one could apply the algorithms to estimate temporal changes.

Northern polar regions: There are clear seasonal differences in both chlorophyll and POC. However, even in winter, POC concentrations appear high off of Alaska, around the British Isles, the Yellow Sea–East China Sea, and the Java Sea. Some of the high values may result from the presence of Case II waters where river runoff and re-suspension of bottom sediments in shallow waters give a false signal of high POC. It is also likely that some regions, particularly in shallower water (Siegel et al., 2002), already have experienced a spring bloom by late March, so the "winter" average is not entirely one of low productivity. The c_p^* values in the northern hemisphere summer are lower (higher productivity) over a much larger region than the austral summer values of the Southern Ocean.

South Atlantic and Southern Ocean: In general the Southern Ocean is an area of high nutrients and relatively low chlorophyll during austral summer. However, there is evidence that the algorithms for chlorophyll concentration based on SeaWiFS data are as much as a factor of two low (Kahru and Mitchell, 1999; Stramska et al., 2003). Chlorophyll values increase significantly in austral summer, especially in the Argentine Basin, Falkland Plateau and along the margin of Antarctica. The elevated

chlorophyll in the Argentine basin coincides with a region of high surface eddy kinetic energy (Cheney et al., 1983; Garraffo et al., 1992; Richardson et al., 1993) that is probably mixing nutrients up into the mixed layer. POC concentrations are highly elevated through most of the Southern Ocean in December–March, but there are large patches where POC and chlorophyll are not high over that 4-month period. The %CHL and c_p^* values in the Southern Ocean exhibit less summer–winter variation than either chlorophyll or POC except along the ice edge or continental margin (once the ice has melted) and in the South Atlantic sector.

The tongue of low-c_p^*, high-POC and high-CHL water starting at South Africa and extending eastward in the Indian Ocean sector of the Southern Ocean is noteworthy, especially during the austral summer (Figs. 7(C), 8(C), 10). The position of that tongue coincides well with the area of the retroflection of the Agulhas Current extending eastward along ~48–52°S. This is a region where drifting buoys revealed persistent eddies moving eastward along that gradient (Pazan and Niiler, 2004). Perhaps the eddies mix up enough useful nutrients to fuel a sustained low level of primary production. The area of high chlorophyll (0.5 mg m^{-3}; Fig. 8(C)) at 50°S and 70°E in the middle of that eastward-extending tongue coincides with the Kerguelen islands, which provide a source of iron and cause island upwelling, thus enhancing productivity in their vicinity. Between South Africa and the Kerguelen Islands and Plateau are the Agulhas Plateau (~2300 m), Prince Edward Island, and the Crozet Plateau and Islands. The circumpolar current moving through and around these obstacles probably causes upwelling all along this line. Similarly, both chlorophyll and POC concentrations are elevated, especially in austral summer in the vicinity and downstream of the South Sandwich Islands east of the Drake Passage.

Coastal regions: Productivity is elevated in coastal regions during both seasons based on the low c_p^* values, but further evaluation is needed to determine the degree to which Case II waters influence the values.

Oligotrophic central gyres of all oceans: The areal extent of low %CHL, high c_p^* values (low productivity, Figs. 7(C), 8(C), 10) in the central gyres of all oceans increases in area and intensity during each hemisphere's "summer". This probably results from summer stratification and lower amounts of nutrients. It is still possible that subsurface chlorophyll maxima exist below these apparently oligotrophic regions as was documented in the Arabian Sea (Gundersen et al., 1998).

Equatorial Pacific: During the May–August period (Fig. 7), the tongue of elevated POC and CHL values are much more constrained along the equator than during December–March (Fig. 8), suggesting more constrained upwelling along the equator. From December–March, CHL abundance along the equator is less pronounced west of 120°W and the region of lower c_p^* values is slightly broader than in May–August.

Seasonal upwelling areas along the west-coast of Africa: The upwelling off of Namibia and off-shore of the Congo River is high in CHL, POC, and %CHL during both summer and winter seasons and exhibit low c_p^* values, suggesting high productivity.

5.2. Aerial coverage by concentration and hemisphere

Histograms of the area of the ocean covered by different POC concentrations (Fig. 11) are divided by hemisphere and season and are based on total area of the ocean. The sums of the histograms are less than 100% and vary by season primarily because of ice cover. Contours and sums are in divisions of 12 for easy conversion to μM (12 mg m^{-3} = 1 μmole l^{-1} or 1 μM). About 80% of the ocean has surface concentrations of less than 72 mg m^{-3} during May–August and about 70% of the ocean is less than 72 mg m^{-3} in December–April. A doubling of the area covered by concentrations of 72–96 mg m^{-3} occurs in the southern hemisphere during the summer with only a slight increase in that area with that concentration in the northern hemisphere. Note that the area covered by the lowest concentration bin (<48 mg m^{-3}) increases from winter to summer in the southern hemisphere because of an increase in the oligotrophic area of the central gyres (Figs. 7(B) and 8(B)), perhaps as a result of stratification and prior utilization of nutrients.

The white lines in Figs. 7(B) and 8(B) are the divisions used by Behrenfeld and Falkowski (1997) in calculating primary productivity by ocean, and are used here to calculate the integrated POC stock in different oceans (Table 3). The Arctic is the region >60°N and the Southern Ocean is >50°S. Table 3 also provides the average annual POC concentration by ocean area. The Atlantic, Pacific and Indian oceans have mean standing stocks of

1.3–1.4 g m^{-2} in the first attenuation depth of the ocean. The accuracy of the data are insufficient to distinguish differences between these three oceans.

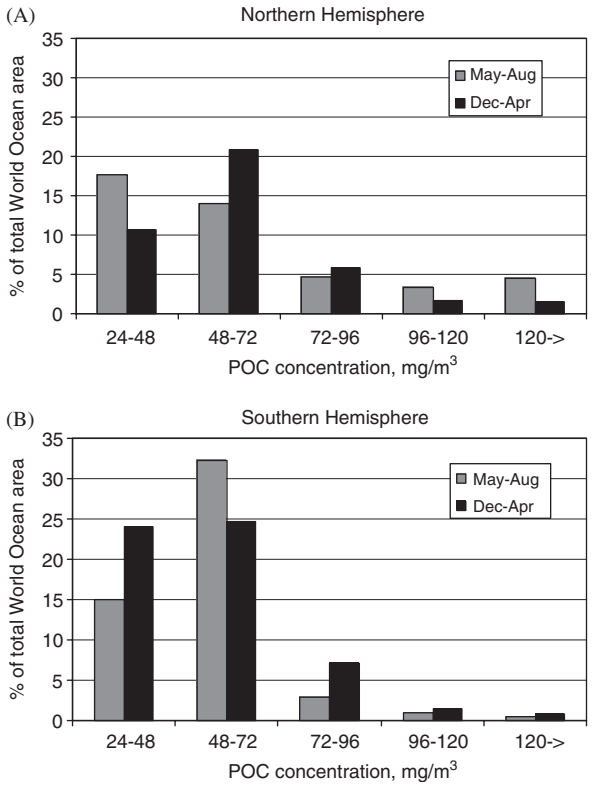

Fig. 11. Histogram of the percent of the total ocean area covered by five ranges of POC concentration in the Northern Hemisphere (A) and Southern Hemisphere (B) in May–August and December–April.

The values for the Arctic (0.4 g m^{-2}) and Southern Ocean (0.8 g m^{-2}) are much smaller, but the algorithm underestimates POC at high latitudes, and overestimates POC in oligotrophic regions, thus making the differences between polar and temperate oceans less certain than the values appear.

Along several WOCE lines in the Pacific we calculated the total POC to the depth when POC reached background levels (based on beam c_p profiles) and determined that the POC in the first attenuation depth is only 20–40% of the total POC down to background levels (Gardner et al., 2003b). This means that the standing stock of POC in the upper ocean could be 2.5–5 times larger than calculated in Table 3. Deep chlorophyll and POC maxima are not sensed by satellites (Gundersen et al., 1998). Although algorithms have been developed to account for deep chlorophyll maxima (Morel, 1988; Sathyendranath et al., 2001), such algorithms remain to be developed for POC.

5.3. Integrated stock and residence time of POC

In estimating the average concentration of POC in the surface attenuation depth of the ocean we also can integrate POC over that depth and obtain a standing stock of POC at each location and calculate contributions by ocean and season. The total global mass of carbon in the first attenuation depth is estimated from our data to be 0.40 Pg C in summer and 0.42 Pg C in winter (Table 3) (Gardner et al., 2003b). If we know the rate of input (primary

Table 3
Regional POC stock ($g \times 10^{13}$) integrated down to one attenuation depth (based on K_{490})

Region	Annual (60 mo avg)	Summer (20 mo avg)	Winter (20 mo avg)	Annual average POC g m^{-2}[a]
Arctic	**0.73**	**0.56**	**0.20**	**0.4**
Atlantic total	**9.82**	**9.54**	**9.41**	**1.3**
N Atlantic	5.76	5.53	5.37	1.2
S Atlantic	4.06	4.01	4.04	1.3
Indian	**7.52**	**7.39**	**7.44**	**1.4**
Pacific total	**19.15**	**18.99**	**18.98**	**1.4**
N Pacific	9.89	9.79	9.71	1.3
NP East	4.47	4.40	4.38	1.4
NP West	5.42	5.39	5.33	1.0
S Pacific	9.26	9.20	9.27	1.4
SP East	2.34	2.32	2.24	1.4
SP West	6.91	6.88	6.93	1.4
Antarctic	**5.61**	**3.94**	**5.52**	**0.8**
Grand total	**42.83**	**40.43**	**41.54**	**1.2**

[a]Annual average POC (g m^{-2}) is the regional stock divided by regional area.

production) or output (export plus remineralization), we can calculate a residence time of POC in surface waters. Behrenfeld and Falkowski (1997) estimated the global annual primary phytoplankton production of POC to be 43.5 Pg C yr^{-1}. Our estimate for the average annual mass of POC in the upper attenuation depth of the ocean from 5 years (1997–2002) of SeaWiFS data is 0.43 Pg C (Table 3), yielding a residence time of 3.6 days. Najjar et al. (2003) estimated the annual export of POC to be 13 Pg C yr^{-1}. Exclusive of remineralization, this yields an approximate residence time of 12 days, which is close to the 18 days (range 8–43 days) estimated at the HOT area in the Pacific (Karl et al., 1996) and 15 days estimated by Eppley et al. (1992) in the same region.

As noted earlier, the POC in the first attenuation depth is 20–40% of the total POC down to background levels (Gardner et al., 2003b). This suggests that the residence time of POC in the upper ocean is 5–2.5 times longer than the time based on one attenuation depth. Calculations of POC stock have been made for each ocean (Table 3), and the residence time in different oceans ranges from 3 to 5 days for one attenuation depth, but 7–12 days if this represents only 40% of the total POC in surface waters and 14–25 days if this represents only 20% of the POC in surface waters. Based on export data of Najjar et al. (2003) the residence time would be 30 days (40%) to 60 days (20%). These preliminary results need further refinement.

5.4. Future applications

Algorithms for POC from ocean-color can be used to make time-series estimates. Doney et al. (2004) point out that this type of data is useful beyond the constraint of model output for spatial distributions and concentrations, citing the example of McClain et al. (1990) where moored current measurements could be used to estimate mass budget values for temporal rate of change, horizontal advective and diffusive fluxes, etc. Such data could be assimilated into numerical models like those of Friedrichs (2002) to optimize model parameters such as growth, mortality and grazing rates to improve our understanding of biological processes and oceanic systems Doney et al. (2004).

The ocean observatories initiatives (e.g., Integrated Ocean Observing System (IOOS), Ocean Observatories Initiative (OOI), Ocean Research Interactive Observatories Networks (ORION)) require that in-situ proxies be created/refined to obtain biogeochemical parameters from relatively easy measurements such as those available with optical devices. Our results are directly applicable to these programs because they provide algorithms to determine POC in the vicinity of these sampling platforms using in-situ optical measurements and enable others to extrapolate the local results to regional or global scales using remotely sensed satellite data.

6. Conclusions

POC concentration can be effectively estimated from beam attenuation data through linear regression of simultaneously collected data. Using ocean-color data collected simultaneously with beam attenuation and POC data in two areas, an empirical relationship between c_p in the surface one attenuation depth of the ocean and K_{490} was developed. A 5-year average of K_{490} during summer and winter seasons was converted to c_p and then to POC using a combined c_p:POC regression. Thus it is possible to predict both POC and chlorophyll concentrations from ocean-color products to assess spatial and temporal variations. If c_p is a better proxy for phytoplankton biomass than POC as suggested by Behrenfeld and Boss (2003), maps of c_p^* provide information about the physiological state of phytoplankton communities, and with other data, predict net primary production Behrenfeld et al. (2005).

Acknowledgments

This work was funded by the NSF Grants OCE-9986762—"Global Synthesis of POC Using Satellite Data Calibrated with Transmissometer and POC Data from JGOFS/WOCE" and OCE-0137171—"Transmissometer Data Validation and Correction for the HOT and BATS Data Sets". The work of colleagues, students and technicians at Texas A&M University who helped collect and analyze portions of these data is greatly appreciated (Dr. Ian Walsh, Dr. Sung Pyo Chung, Bret Berglund, Christina Bernal, Jan Gundersen, Josh Blakey, Sarah Searson, Chris Nugent, Richard Weitz). We thank the many technicians and scientists from the JGOFS, WOCE and SAVE programs for assisting in our participation in these cruises. Help from personnel at the SIO Ocean Data Facility (especially Carl Mattson, Mary Johnson, Bob Williams, and

Dr. Jim Swift) was particularly valuable. We also thank three reviewers for useful remarks and comments. This is JGOFS publication # 1046.

References

Aiken, J., Cummings, D.G., Gibb, S.W., Rees, N.W., Woodd-Walker, R., Woodward, E.M.S., Woolfenden, J., Hooker, S.B., Berthon, J-F., Dempsey, C.D., Suggett, D.J., Wood, P., Donlon, C., Gonzalez-Benitez, N., Huskin, I., Quevedo, M., Barciela-Fernandez, R., de Vargas, C., McKee, C., 1998. AMT-5 Cruise Report. In: Hooker, S.B., Firestone, E.R. (Eds.), NASA Technical Memorandum 1998–206892, vol. 2. NASA Goddard Space Flight Center, Greenbelt, MD (113pp).

Banse, K., 1977. Determining the carbon-to-chlorophyll ration of natural phytoplankton. Marine Biology 41, 199–212.

Bartz, R., Zaneveld, J.R.V., Pak, H., 1978. A transmissometer for profiling and moored observations in water. SPIE 160; Ocean Optics V, 102–108.

Behrenfeld, M.J., Boss, E., 2003. The beam attenuation to chlorophyll ratio: an optical index of phytoplankton physiology in the surface ocean? Deep-Sea Research I 50, 1537–1549.

Behrenfeld, M.J., Falkowski, P.G., 1997. Photosynthetic rates derived from satellite-based chlorophyll concentration. Limnology and Oceanography 42 (1), 1–20.

Behrenfeld, M.J., Boss, E., Siegel, D.A., Shea, D.M., 2005. Carbon-based ocean productivity and phytoplankton physiology from space. Global Biogeochemical Cycles 19, GB1006.

Bernal, C.E., 2001. Spatial and temporal distributions of particulate matter and particulate organic carbon, Northeast Gulf of Mexico. M.Sc.Thesis, Texas A&M University.

Bishop, J.K.B., 1986. The correction and suspended particulate matter calibration of Sea Tech transmissometer data. Deep-Sea Research I 33, 121–134.

Bishop, J.K.B., 1999. Transmissometer measurement of POC. Deep-Sea Research I 46 (2), 353–369.

Bishop, J.K.B., Calvert, S.E., Soon, M.Y.S., 1999. Spatial and temporal variability of POC in the northeast Subarctic Pacific. Deep-Sea Research II 46 (11–12), 2699–2733.

Bishop, J.K.B., Davis, R.E., Sterman, J.T., 2002. Robotic observation of dust storm enhancement of carbon biomass in the North Pacific. Science 298, 817–821.

Bishop, J.K.B., Wood, T.J., Davis, R.E., Sterman, J.T., 2004. Robotic observation of enhanced carbon biomass at 55°S during SOFeX. Science 304, 417–420.

Boss, E., Twardowski, M.S., Herring, S., 2001. Shape of the particulate beam attenuation spectrum and its inversion to obtain the shape of the particulate size distribution. Applied Optics 40, 4885–4893.

Bricaud, A., Morel, A., Prieur, L., 1981. Absorbtion by dissolved matter of the sea (yellow substance) in the UV and visible domains. Limnology and Oceanography 26, 43–53.

Campbell, J.W., Blaisdell, J.M., Darzi, M., 1995. Level-3 SeaWiFS data products: spatial and temporal binning algorithms. SeaWiFS Technical Report Series 32, 73.

Carr, M.E., Friedrichs, M.A.M., Schmeltz, M., Aita, M.N., Antoine, D., Arrigo, K.R., Asanuma, I., Aumont, O., Barber, R., Behrenfeld, M., Bidigare, R., Buitenhuis, E.T., Campbell, J., Coitti, A., Dierssen, H., Dowell, M., Dunne, J., Esaias, W., Gentili, B., Gregg, W., Groom, S., Hoepffner, N., Ishizaka, J., Kameda, T., LeQuere, C., Lohrenz, S., Marra, J., Melin, F., Moore, J.K., Morel, A., Reddy, T.E., Ryan, J., Scardi, M., Smyth, T., Turpie, K., Tilstone, G., Waters, K., Yamanaka, Y., 2006. A comparison of global estimates of marine primary production from ocean color. Deep-Sea Research II, this volume [doi: 10.1016/j.dsr2.2006.01.029].

Cheney, R.E., Marsh, I.G., Beckley, B.O., 1983. Global mesoscale variability from colinear tracks of SEASAT altimeter data. Journal of Geophysical Research 88, 4343–4354.

Chipman, D.W., Marra, J., Takahashi, T., 1993. Primary production at 47N and 20W in the North Atlantic Ocean: a comparison between the ^{14}C incubation method and the mixed layer carbon budget. Deep-Sea Researh II 40, 151–169.

Chung, S.P., Gardner, W.D., Richardson, M.J., Walsh, I.D., Landry, M.R., 1996. Beam attenuation and microorganisms: spatial and temporal variations in small particles along 140°W during 1992 JGOFS–EqPac transects. Deep-Sea Research II 43, 1205–1226.

Chung, S.P., Gardner, W.D., Landry, M.R., Richardson, M.J., Walsh, I.D., 1998. Beam attenuation my microorganisms and detrital particles in the Equatorial Pacific. Journal of Geophysical Research—Oceans 104 (C2), 3401–3422.

Christian, J.R., Verschell, M.A., Murtugudde, R., Busalacchi, A.J., McClain, C.R., 2002. Biogeochemical modelling of the tropical Pacific Ocean, 2002 I: seasonal and interannual variability. Deep-Sea Research II 49 (1–3), 509–543.

Claustre, H., Morel, A., Babin, M., Cailliau, C., Marie, D., Marty, J.-C., Tailliez, D., Vaulot, D., 1999. Variability in particle attenuation and chlorophyll fluorescence in the Tropical Pacific: scales, patterns, and biogeochemical implications. Journal of Geophysical Research 104 (C2), 3401–3422.

Del Castillo, C.E., Coble, P.G., Conmy, R.N., Muller-Karger, F.E., Vanderbloemen, L., Vargo, G.A., 2001. Multispectral in situ measurements of organic matter and chlorophyll fluorescence in seawater: documenting the intrusion of the Mississippi River plume in the West Florida Shelf. Limnology and Oceanography 46 (7), 1836–1843.

Deuser, W.G., Brewer, P.G., Jickells, T.D., Commeau, R.F., 1983. Biological control of the removal of abiogenic particles from the surface ocean. Science 219, 388–391.

Doney, S.C. (Ed.) and 18 co-authors, 2004. Ocean carbon and climate change: an implementational strategy for US ocean carbon research. Report for US CCSSG & CCIWG.

DuRand, M.D., Olson, R.J., 1996. Contributions of phytoplankton light scattering and cell concentration changes to diel variations in beam attenuation in the equatorial Pacific from flow cytometric measurements of pico-, ultra- and nanoplankton. Deep-Sea Research II 43, 891–906.

El-Sayed, S.Z., Taguchi, S., 1981. Primary production and standing crop of phytoplankton along the ice-edge in the Weddel Sea. Deep-Sea Research 28, 1017–1032.

Eppley, R.W., Harrison, W.G., Chisholm, S.W., Stewart, E., 1977. Particulate organic matter in surface waters off Southern California and its relationship to phytoplankton. Journal of Marine Research 35, 671–696.

Eppley, R.W., Chavez, F.P., Barber, R.T., 1992. Standing stocks of particulate carbon and nitrogen in the equatorial Pacific at 150°W. Journal of Geophysical Research 97, 655–661.

Evans, R., Minnett, P., Brown, O., Kumar, A., Kilpatrick, K., Kearns, E., 2000. Early results from NASA's moderate resolution scanning spectrometer (MODIS): Global and Arabian Sea regional ocean color and thermal observations. In: Proceedings of the Fifth Pacific Ocean Remote Sensing Conference (PORSEC). National Institute of Oceanography, Dona Paula, Goa, India, vol.1, p. 5.

Feely, R.A., Sabine, C.L., Schlitzer, R., Bullister, J.L., Mecking, S., Greeley, D., 2004. Oxygen utilization and organic carbon remineralization in the upper water column of the Pacific Ocean. Journal of Oceanography 60 (1), 45–52.

Fennel, K., Boss, E., 2003. Subsurface maxima of phytoplankton and chlorophyll steady state solutions from a simple model. Limnology and Oceanography 48, 1521–1534.

Friedrichs, M.A.M., 2002. Assimilation of JGOFS EqPac and SeaWiFS data into a marine ecosystem model of the central equatorial Pacific Ocean. Deep-Sea Research II 49, 289–319.

Gardner, W.D., 1989. Baltimore Canyon as a modern conduit of sediment to the deep sea. Deep-Sea Research 36, 323–358.

Gardner, W.D., Biscaye, P.E., Zaneveld, J.R.V., Richardson, M.J., 1985. Calibration and comparison of the LDGO nephelometer and the OSU transmissometer on the Nova Scotian rise. Marine Geology 66, 323–344.

Gardner, W.D., Walsh, I.D., Richardson, M.J., 1993. Biophysical forcing of particle production and distribution during a spring bloom in the North Atlantic. Deep-Sea Research II 40, 171–195.

Gardner, W.D., Chung, S.P., Richardson, M.J., Walsh, I.D., 1995. The oceanic mixed-layer pump. Deep-Sea Research II 42, 757–775.

Gardner, W.D., Gundersen, J.S., Richardson, M.J., Walsh, I.D., 1999. The role of diel variations in mixed-layer depth on the distribution, variation, and export of carbon and chlorophyll in the Arabian Sea. Deep-Sea Research II 46, 1833–1858.

Gardner, W.D., Richardson, M.J., Smith, W.O., 2000a. Seasonal patterns of water column particulate organic carbon and fluxes in the Ross Sea, Antarctica. Deep-Sea Research II 47 (15–16), 3423–3449.

Gardner, W.D., Richardson, M.J., Walsh, I.D., Smith, W.O., 2000b. POC Variations and Physical Forcing in the Antarctic Polar Front Zone During Spring–Fall, 1997–1998. Ocean Sciences, San Antonio, TX, p. 199.

Gardner, W.D., Blakey, J.C., Walsh, I.D., Richardson, M.J., Pegau, S., Zaneveld, J.R.V., Roesler, C., Gregg, M.C., MacKinnon, J.A., Sosik, H.M., Williams, A.J., 2001. Optics, particles, stratification, and storms on the New England continental shelf. Journal of Geophysical Research—Oceans 106 (C5), 9473–9497.

Gardner, W.D., Richardson, M.J., Carlson, C.A., Hansell, D., Mishonov, A.V., 2003a. Determining true particulate organic carbon: bottles, pumps and methodologies. Deep-Sea Research II 50 (3–4), 655–674.

Gardner, W.D., Mishonov, A.V., Richardson, M.J., 2003b. Global POC distribution using Ocean Color and WOCE/JGOFS Beam Attenuation and POC Data. EGS—AGU—EUG Joint Assembly, Nice, France.

Garraffo, Z.S., Garzzoli, W., Haxby, W., Olson, D., 1992. Analysis of a general circulation model, part 2: the distribution of kinetic energy in the South Atlantic and in the Kuroshio–Oyashimo system. Journal of Geophysical Research 97, 20139–20153.

Geider, R.J., MacIntyre, H.L., Kana, T.M., 1998. A dynamic regulatory model of phytoplanktonic acclimation to light, nutrients, and temperature. Limnology and Oceanography 43 (4), 679–694.

Gordon, H.R., McCluney, W.R., 1975. Estimation of the depth of sunlight penetration in the sea for remote sensing. Applied Optics 14 (2), 413–416.

Green, R.E., Sosik, H.M., 2004. Analysis of apparent optical properties and ocean color models using measurements of seawater constituents in New England continental shelf surface waters. Journal of Geophysical Research, 109, doi:10.1029/2003JC001977.

Green, R.E., Sosik, H.M., Olson, R.J., 2003. Contributions of phytoplankton and other particles to inherent optical properties in New England continental shelf waters. Limnology and Oceanography 48, 2377–2391.

Gundersen, J.S., Gardner, W.D., Richardson, M.J., Walsh, I.D., 1998. Effects of monsoons on the seasonal and spatial distribution of POC and chlorophyll in the Arabian Sea. Deep-Sea Research II 45, 2103–2132.

Gundersen, K., Orcutt, K.M., Purdie, D.A., Michaels, A.F., Knap, A.H., 2001. Particulate organic carbon mass distribution at the Bermuda Atlantic Time-series Study (BATS) site. Deep-Sea Research II 48 (8–9), 1697–1718.

Hebel, D.V., Karl, D.M., 2001. Seasonal, interannual and decadal variations in particulate matter concentrations and composition in the subtropical North Pacific Ocean. Deep-Sea Research II 48, 1669–1695.

Hood, R.R., Kohler, K.E., McCreary Jr., J.P., Smith, S.L., 2003. A four-dimensional validation of a coupled physical–biological model of the Arabian Sea. Deep-Sea Research II 50 (22–26), 2917–2945.

Hooker, S.B., McClain, C.R., 2000. The calibration and validation of SeaWiFS data. Progress in Oceanography 45 (3–4), 427–465.

Jackson, G.A., Burd, A.B., 2002. A model for the distribution of particle flux in the mid-water column controlled by subsurface biotic interactions. Deep-Sea Research II 49 (1–3), 193–217.

JGOFS, 1996. Protocols for the Joint Global Ocean Flux Study (JGOFS) core measurements. Report #19, Intergovernmental Oceanographic Commission, Bergen, Norway (170pp).

Kahru, M., Mitchell, B.G., 1999. Empirical chlorophyll algorithm and preliminary SeaWiFS validation for the California Current. International Journal of Remote Sensing 20, 3423–3429.

Kahru, M., Marinone, S.G., Lluch-Cota, S.E., Pares-Sierra, A., Mitchell, B.G., 2004. Ocean-color variability in the Gulf of California: scales from days to ENSO. Deep-Sea Research II 51, 139–146.

Karl, D.M., Lukas, R., 1996. The Hawaii Ocean Time-series (HOT) program: background, rationale and field implementation. Deep-Sea Research II 43 (2–3), 129–156.

Karl, D.M., Christian, J.R., Dore, J.E., Hebel, D.V., Letelier, R.M., Tupas, L.M., Winn, C.D., 1996. Seasonal and interannual variability in primary production and particle flux at Station ALOHA. Deep-Sea Research II 43 (2–3), 539–568.

Kitchen, J., Zaneveld, J.R.V., 1990. On the noncorrelation of the vertical structure of light scattering and chlorophyll a in case I waters. Journal of Geophysical Research 95, 20,237–20,246.

Knap, A.H., Michaels, A.F., Close, A., 1994. The JGOFS Protocols. Intergovernmental Oceanographic Commission, 198pp.

Landry, M.R., Barber, R.T., Bidigare, R.R., Chai, F., Coale, K.H., Dam, H.G., Lewis, M.R., Lindley, S.T., McCarthy, J.J., Roman, M.R., Stoecker, D.K., Verity, P.G., White, J.R., 1997. Iron and grazing constraints on primary production in the Central Equatorial Pacific: an EqPac synthesis. Limnology and Oceanography 42 (3), 405–418.

Le Borgne, R., Feely, R., Mackey, D., 2002. Carbon fluxes in the equatorial Pacific: a synthesis of the JGOFS programme. Deep-Sea Research II 49 (13–14), 2425–2442.

Lee, C., Murray, D.W., Barber, R.T., Buesseler, K.O., Dymond, J., Hedges, J.I., Honjo, S., Manganini, S.J., Marra, J., Moser, C., Peterson, M.L., Prell, W.L., Wakeham, S.G., 1998. Particulate organic carbon fluxes: compilation of results from the 1995 US JGOFS Arabian Sea Process Study. Deep-Sea Research II 45, 2489–2501.

Legendre, L., Michaud, J., 1999. Chlorophyll a to estimate the particulate organic carbon available as food to large zooplankton in the euphotic zone of oceans. Journal of Plankton Research 21 (11), 2067–2083.

Lewis, M.R., Cullen, J.J., Platt, T., 1983. Phytoplankton ant thermal structure in the upper ocean: consequences of nonuniformity in chlorophyll profile. Journal of Geophysics Research 88, 2565–2570.

Liu, Z.F., Stewart, G., Cochran, J.K., Lee, C., Armstrong, R.A., Hirschberg, D.J., Gasser, B., Miquel, J.-C., 2005. Why do POC concentrations measured using Niskin bottle collections sometimes differ from those using in-situ pumps? Deep-Sea Research Part I—Oceanographic Research Papers 52, 1324–1344.

Loisel, H., Boss, E., Stramski, D., Oubelkheir, K., Deschamps, P.Y., 2001. Seasonal variability of the backscattering coefficient in the Mediterranean Sea based on Satellite SeaWiFS imagery. Geophysical Research Letters 28 (22), 4203–4206.

MacCready, P., Quay, P., 2001. Biological export flux in the Southern Ocean estimated from a climatological nitrate budget. Deep-Sea Research 49, 4299–4322.

McClain, C.R., Ishizaka, J., Hofmann, E., 1990. Estimation of phytoplankton pigment changes of the Southeastern U.S. continental shelf from a sequence of CZCS images and a coupled physical–biological model. Journal of Geophysics Research 95 (C11), 20213–20235.

Menzel, D.W., 1967. Particulate organic carbon in the deep sea. Deep-Sea Research 14, 229–238.

Mishonov, A.V., Gardner, W.D., 2003a. Assessment and correction of the historical beam attenuation data from HOT—ALOHA & BATS sites. Oceanography 16 (2), 51.

Mishonov, A.V., Gardner, W.D., Richardson, M.J., 2003b. Remote sensing and surface POC concentration in the South Atlantic. Deep-Sea Research II 50 (22–26), 2997–3015.

Mitchell, B.G., Kiefer, D.A., 1988. Variability in pigment specific particulate fluorescence and absorption spectra in the northeastern Pacific Ocean. Deep-Sea Research 35, 665–689.

Mitchell, B.G., Holm-Hansen, O., 1991. Bio-optical properties of Antarctic Peninsula waters differentiation from temperate ocean models. Deep-Sea Research 38, 1009–1028.

Moran, S.B., Charette, M.A., Pike, S.M., Wickland, C.A., 1999. Differences in seawater particulate organic carbon concentration in samples collected using small-volume and large-volume methods: the importance of DOC absorption to the filter blank. Marine Chemistry 67, 33–42.

Morel, A., 1988. Optical modelling of the upper ocean in relation to its biogenous matter content (Case I Waters). Journal of Geophysical Research 93 (C9), 10749–10768.

Morel, A., Berthon, J.F., 1989. Surface pigments, algal biomass profiles and potential production of the euphotic layer: relationships investigated in view of remote-sensing applications. Limnology and Oceanography 34, 1545–1562.

Morel, A., Maritorena, S., 2001. Bio-optical properties of oceanic waters: a reappraisal. Journal of Geophysical Research 106 (C4), 7163–7180.

Morel, A., Prieur, L., 1977. Analysis of variations in ocean color. Limnology and Oceanography 22 (4), 709–722.

Morrison, J., Gaurin, S., Codispoti, L.A., Takahashi, T., Millero, F.J., Gardner, W.D., Richardson, M.J., 2001. Seasonal evolution of the hydrographic properties during the Antarctic Circumpolar Current at 170°W during 1997–1998. Deep-Sea Research II 48, 3943–3972.

Najjar, R.G., Jin, X., Louanchi, F., Aumont, O., Caldeira, K., Doney, S.C., Dutay, J.-C., Fallows, M., Kay, G.M., Maier-Reimer, E., Matear, R.J., Mouchet, A., Orr, J.C., Plattner, G.K., Sarmiento, J.L., Weirig, M.F., Yamanak, Y., Yool, A., 2003. Export production simulated by the OCMIP-2 models. JGOFS Open Science Conference, Washington, DC, 5–8 May 2003.

Nelson, D.M., Anderson, R.F., Barber, R.T., Brzezinski, M.A., Buesseler, K.O., Chase, Z., Collier, R.W., Dickson, M.L., François, R., Hiscock, M.R., Honjo, S., Marra, J., Martin, W.R., Sambrotto, R.N., Sayles, F.L., Sigmon, D.E., 2002. Vertical budgets for organic carbon and biogenic silica in the Pacific Sector of the Southern Ocean, 1996–1998. Deep-Sea Research II 49, 1645–1674.

Pak, H., Menzies, D., Zaneveld, J.R.V., 1988. Optical and Hydrographical observations of the coast of Peru during May–June 1977. Naval Report 083–102 N00014-76*0067. University of Oregon.

Pazan, S.E., Niiler, P., 2004. New global drifter data set available. AGU-Eos 85 (2), 17.

Richardson, M.J., Weatherly, G.L., Gardner, W.D., 1993. Benthic storms in the Argentine Basin. Deep-Sea Research 40, 957–987.

Richardson, M.J., Gardner, W.D., Smith, W.O., 1999. Seasonal and Spatial Variability in POC Distributions in the Ross Sea. ASLO, Santa Fe, NM.

Richardson, M.J., Gardner, W.D., Mishonov, A.V., Son, Y.B., 2003. Particulate Organic carbon in the North-East Gulf of Mexico: developing algorithms between bio-optical data and satellite ocean color products. Oceanography 16 (2), 57.

Sabine, C.L., Key, R.M., Feely, R.A., Greeley, D., 2002. Inorganic carbon in the Indian Ocean: distribution and dissolution processes. Global Biogeochemical Cycles 16(4), Art. #1067.

Sathyendranath, S., Platt, T., 1997. Analytic model of ocean color. Applied Optics 36 (12), 2620–2629.

Sathyendranath, S., Platt, T., Stuart, V., 2000. Remote sensing of ocean colour: Recent advances, exciting possibilities and unanswered questions. In: Proceedings of the Fifth Pacific Ocean Remote Sensing Conference (PORSEC), National Institute of Oceanography, Dona Paula, Goa, India, vol. 1, p. 6.

Sathyendranath, S., Cota, G., Stuart, V., Maass, H., Platt, T., 2001. Remote sensing of phytoplankton pigments: a comparison of empirical and theoretical approaches. International Journal of Remote Sensing 22 (2–3), 249–273.

Schlitzer, R., 2002. Carbon export fluxes in the Southern Ocean: results from inverse modeling and comparison with satellite-based estimates. Deep-Sea Research II 49 (9–10), 1623–1644.

Schlitzer, R., 2003. Ocean Data View, http://www.awi-bremerhaven.de/GEO/ODV.

Shifrin, K.S., 2001. An algorithm for determining the radiance reflected from the rough sea surface using MODIS-N satellite radiometer data. IEEE Transactions on Geoscience and Remote Sensing 39 (3), 677–681.

Siegel, D.A., Doney, S.C., Yoder, J.A., 2002. The North Atlantic spring phytoplankton bloom and Sverdrup's critical depth hypothesis. Science 296, 730–733.

Smith Jr., W.O., Nelson, D.M., DiTullio, G.R., Leventer, A.R., 1996. Temporal and spatial patterns in the Ross Sea: phytoplankton biomass, elemental composition, productivity and growth rates. Journal of Geophysics Research 101, 18,455–18,466.

Smith Jr., W.O., Marra, J., Hiscock, M.R., Barber, R.T., 2000. The seasonal cycle of phytoplankton biomass and primary productivity in the Ross Sea, Antarctica. Deep-Sea Research II 47, 3119–3140.

Spinrad, R.W., 1986. A calibration diagram of specific beam attenuation. Journal of Geophysical Research 91, 7761–7764.

Spinrad, R.W., Zaneveld, J.R.V., Kitchen, J.C., 1983. A study of the optical characteristics of the suspended particles in the benthic nepheloid layer of the Scotian Rise. Journal of Geophysical Research 88 (C12), 7641–7645.

Steinberg, D.K., Carlson, C.A., Bates, N.R., Johnson, R.J., Michaels, A.F., Knap, A.H., 2001. Overview of the US JGOFS Bermuda Atlantic Time-series Study (BATS): a decade-scale look at ocean biology and biogeochemistry. Deep-Sea Research II 48 (8–9), 1405–1448.

Stramska, M., Stramski, D., Hapter, R., Kaczmarek, S., Ston, J., 2003. Bio-optical relationships and ocean color algorithms for the north polar region of the Atlantic. Journal of Geophysical Research 108 (C5), 3143.

Stramski, D., Kiefer, D., 1991. Light scattering by microorganizms in the open ocean. Progress in Oceanography 28, 343–383.

Stramski, D., Reynolds, R.A., Kahru, M., Mitchell, B.G., 1999. Estimation of particulate organic carbon in the ocean from satellite remote sensing. Science 285 (5425), 239–242.

Twardowski, M.S., Boss, E., Macdonald, J.B., Pegau, W.S., Barnard, A.H., Zaneveld, J.V.R., 2001. A model for estimating bulk refractive index from the optical backscattering ratio and the implication for understanding particle composition in case I and case II waters. Journal of Geophysics Research—Oceans 106 (C7), 14129–14142.

Walsh, I.D., Chung, S.P., Richardson, M.J., Gardner, W.D., 1995. The diel cycle in the integrated particle load in the equatorial Pacific: a comparison with primary production. Deep-Sea Research II 42, 465–477.

Walsh, I.D., Gardner, W.D., Richardson, M.J., Chung, S.-P., Plattner, C.A., Asper, V., 1997. Particle dynamics as controlled by the flow field of the Eastern Equatorial Pacific. Deep-Sea Research II 44, 2025–2047.

Zaneveld, J.R.V., 1973. Variation of optical sea water parameters with depth. In: Optics of the Sea Interface and In-Water Transmission and Imagery, NATO Lecture Series, vol. 61, pp.1–22.